POLITECNICO DI TORINO
Repository ISTITUZIONALE

Adoption of simplified parabolic trough collectors for domestic hot water applications: numerical and experimental investigation

Original
Adoption of simplified parabolic trough collectors for domestic hot water applications: numerical and experimental investigation / Mahdhi, J., Ebadi, H., Bouabidi, A., Ennetta, R., Savoldi, L.. - In: CASE STUDIES IN THERMAL ENGINEERING. - ISSN 2214-157X. - (2026). [10.1016/j.csite.2026.108693]

Availability:
This version is available at: 11583/3017517 since: 2026-11-04T13:46:15Z

Publisher:
Case Studies in Thermal Engineering

Published
DOI:10.1016/j.csite.2026.108693

Terms of use:

This article is made available under terms and conditions as specified in the corresponding bibliographic description in the repository

Publisher copyright

(Article begins on next page)

28 November 2026

Case Studies in Thermal Engineering 88 (2026) 108693

Contents lists available at ScienceDirect

Case Studies in Thermal Engineering

journal homepage: www.elsevier.com/locate/csite

Adoption of simplified parabolic trough collectors for domestic hot water applications: numerical and experimental investigation

Jihen Mahdhi [a,b], Hossein Ebadi [a,*], Abdallah Bouabidi [b], Ridha Ennetta [b], Laura Savoldi [a]

[a] MAHTEP Group, Dipartimento Energia "Galilo Ferraris" (DENERG), Politecnico di Torino, 10129, Turin, Italy
[b] Laboratory of Mechanical Modeling, Energy and Materials (LM2EM), National Engineering School of Gabes, University of Gabes, 6029, Gabes, Tunisia

GRAPHICAL ABSTRACT

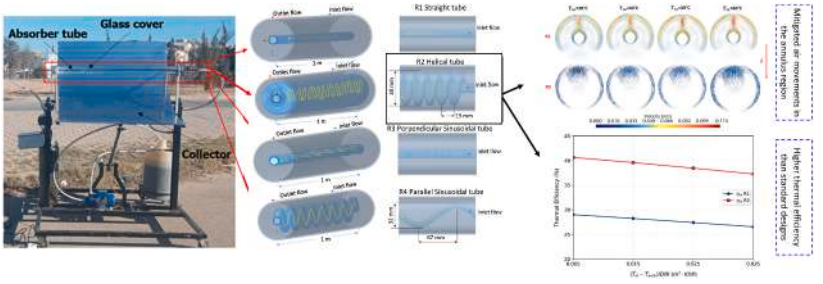

ARTICLE INFO

Keywords:
Parabolic trough collector
Non-evacuated receiver
Absorber tube geometry
Helical and sinusoidal tubes
Thermo-hydraulic performance
CFD

ABSTRACT

Compared to evacuated systems, stationary and non-evacuated parabolic trough collectors (PTCs) are less expensive and require less maintenance, making them a potential option for home hot water applications. But without vacuum insulation and sun tracking, thermal heat losses increase and efficiency declines. This study proposes tube geometry modification for a low-cost, small-scale, non-tracking, and non-evacuated PTC to overcome these limitations. A simple (R1), a helical tube (R2), and sinusoidal tubes oriented perpendicular (R3) and parallel (R4) are examined to adopt this technology for hot water production systems. Using a combination of numerical and experimental methods, 3D Computational Fluid Dynamics (CFD) simulations are coupled with Monte Carlo Ray Tracing (MCRT) optical analysis. After the validation of numerical models against experimental data, CFD results are used to compare the performance of various geometries. Results revealed the distinct role of receiver geometry in driving air movements between the

* Corresponding author.
E-mail address: hossein.ebadi@polito.it (H. Ebadi).

https://doi.org/10.1016/j.csite.2026.108693
Received 17 June 2026; Received in revised form 24 October 2026; Accepted 29 October 2026
2214-157X/© 2026 The Authors. Published by Elsevier Ltd. This is an open access article under the CC BY-NC-ND license (http://creativecommons.org/licenses/by-nc-nd/4.0/).

tube and the glass cover. Moreover, all the modified receivers reflect an increased thermal performance compared to the conventional tube design, while the pressure drop penalty also increases. The helical receiver displays the strongest internal fluid mixing, achieving the maximum water outlet temperature rise. Moreover, the R2 tube outperformed other designs, achieving the maximum thermal efficiency of 40% and exergy efficiency of 2%. In addition, the helical receiver improves the average *Nu* by 360% and the overall efficiency by 38.6% compared to the simple design. As a result, the helical receiver was selected as the optimum design for boosting the efficiency of the stationary non-evacuated PTC system.

1. Introduction

The increasing global energy demand, together with the urgent need to mitigate climate change impacts, has significantly accelerated the deployment of renewable energy technologies [1]. Along with space heating, Domestic Hot Water (DHW) production is one of the main energy-consuming home applications that accounts for 79% of energy demand in the building sector [2]. Although space heating varies depending on the seasonal conditions, DHW demand remains stable during the year and still highly depends on fossil fuels [3].

Decarbonization of residential DHW systems is becoming viable through the implication of renewable energy technologies such as solar water heating systems. Recent studies [4] have shown that the deployment of solar thermal power systems for residential buildings decreases the annual auxiliary energy consumption by 2863 kWh. This translates to a total lifetime CO_2 emissions reduction with a range of approximately 11.6 to 25.2 tons. Other studies [5] demonstrated that a standalone solar thermal energy system can provide 75% of the hot water consumption needs. Flat plate and evacuated tube collectors are the two main technologies commonly used in previous studies [6]. Recently, small-scale Parabolic Trough Collectors (PTC) have emerged as a new solution for DHW production in industrial, domestic and rural applications thanks to their high thermal performance [7].

PTC systems work by focusing Direct Normal Irradiance (DNI) onto a linear receiver that is positioned parallel to a parabolic reflector's focal line. The Heat Transfer Fluid (HTF) that flows through the receiver tube carries the absorbed solar thermal power and transfers it to the industrial thermal processes or to make electricity through traditional steam cycles. In order to adopt this technology for domestic applications, where skilled operators are scarce and no continuous observation is needed, PTC should be simplified in terms of design, operation and maintenance [8]. As a result, making them stationary and non-evacuated would be two major revisions applied to the simplified PTCs [9]. Knowing that these amendments would reduce PTC thermal efficiency and downgrade its performance for long-term operations, the implementation of one or multiple thermal enhancements is necessary.

Absorber tube geometry modification has been proposed in a large amount of literature as a successful technique to enhance PTC thermal performance. This strategy aimes at improving fluid mixing and increasing the effective heat transfer surface area through U-shaped, sinusoidal, helical (spiral), and other non-linear geometries [10]. In an experimental analysis, Kumar and Shukla [11] analyzed a PTC system equipped with a helical coil cavity receiver to improve heat transfer and reduce thermal losses. Nevertheless, their study highlighted the system's sensitivity to vacuum quality, reporting a 26.67% increase in heat loss following a 50% increase in vacuum pressure. Vengadesan et al. [12] demonstrated experimentally that a 7 mm semicircular absorber with two inlets works noticeably better (rise in heat transfer coefficient and thermal efficiency of 28.5% and 43.9%, respectively) than standard 25 mm circular versions, due to an enlarged flow path and decreased hydraulic diameter. Halimi et al. [13] investigated a PTC equipped with a U-shaped tube heat exchanger and demonstrated that aligning the U-tube parallel to the absorber axis yields a thermal efficiency of roughly 40%. Similarly, comparing a helical straight-flow U-tube design with a standard U-tube in vacuum tube collectors, Essa et al. [14] found that the former had a 6.1% energy efficiency while the latter had a 3.8%. Gholipour et al. [15] experimentally discovered that the helical coil outperforms helical tubes and U-tubes, leading the PTC to reach efficiencies above 58%. Lotake et al. [16] reported an increase in efficiency (about 15–31%) when using several helical tubes as PTC receivers. In their experimental evaluation of helically corrugated absorber tubes with varying pitch ratios, Akbarzadeh and Valipour [17] confirmed the high potential of surface alterations to improve PTC efficiency by exhibiting a Nusselt number enhancement of almost four. Sunkarwar et al. [18] investigated a parallel-flow evacuated U-tube solar collector with a parabolic reflector under hot tropical conditions, reporting that thermal efficiency dropped to 66% in the absence of particulate matter. Bayhan et al. [19] examined a natural circulation solar system with a parabolic trough collector and found that 56% of the incoming radiation entered the vacuum tube glass pipe in the collector's focus. Hameed et al. [20] assessed a helical receiver for PTCs at various water flow rates, finding a notable improvement in thermal performance with a maximum efficiency of 69.4%. This study indicates that helical receivers require less available space to gain the same amount of heat compared to the traditional PTCs, which leads to minimal construction and foundation costs. Furthermore, they demonstrated that helical coils introduce curvature and a centrifugal force on the flowing fluid, causing secondary flow (Dean vortices), enhancing mixing, and increasing the heat transfer coefficient. Dengre et al. [21] tested a 2.8 m^2 PTC collector with helical coil receivers and achieved a maximum receiver thermal efficiency of 85.4%, which suggested this design as an efficient and durable configuration for residential PTCs.

In parallel, numerous researchers have employed a numerical approach to study the influence of absorber tube geometry on PTC performance. Oumachtaq et al. [22] analyzed three alternative receiver configurations and found that the helical tube provided the highest outlet temperature and thermal efficiency, exceeding 90% at high flow rates and low inlet temperatures. Helical absorber tubes were also addressed by Chakrabort et al. [23], revealing that *Nu* increases by 25% due to a rise in flow turbulence, where the fluid

intermixing enhances and causes uniform temperature distribution inside the PTC absorber tube. In another study, Said et al. [24] proposed PTCs with a helical absorber for DHW systems and achieved a maximum thermal efficiency of 72% through a numerical investigation. Ebadi et al. [25] proposed a novel receiver design, featuring a multi-tube cavity instead of a simple tube absorber to reduce the size of thermal boundary layers and increase turbulence in fluid streams, which resulted in a 7% higher overall efficiency. In order to improve heat transfer by generating vortices in the fluid stream, Byiringiro et al. [26] used a Computational Fluid Dynamics (CFD) tool to numerically study novel PTC receivers with internal fins. Mustafa et al. [27] numerically examined a double-fluid PTC equipped with a helical absorber tube, demonstrating that the increased surface area and induced turbulence significantly enhance heat transfer. Loni and Sharifzadeh [28] examined several linear cavity receiver layouts, such as trapezoidal, V-shaped, and cubical designs, and demonstrated that the cubical receiver performed the best. Saini et al. [29] investigated the use of a uniform helical wire coil insert, observing enhanced heat transfer with only a minor increase in pressure drop. Shi et al. [30] demonstrated that a helically convex absorber tube can increase overall heat transfer by more than 30%. By increasing both heat transfer surface area and fluid turbulence, Bellos et al. [31] analyzed the fluid flow and heat transmission in a concave sinusoidal absorber tube to enhance thermal performance. Finally, in another analysis of the major factors influencing PTC performance, Naveenkumar et al. [32] highlighted that sinusoidal absorbers and asymmetric external corrugated pipes have great potential for integration with future non-evacuated PTCs. Iliquin-Fernandez et al. [33] investigated how absorber tube shape influences the thermal performance of PTCs for DHW. Their study revealed that the triangle absorber design outperforms the standard linear structure, reaching a thermal efficiency of 44.12% while increasing hot water production by around 35% due to better heat transmission.

Considering that most of the experimental and numerical studies surveyed above focus on geometry alteration in large-scale PTC systems or evacuated receivers, where vacuum insulation efficiently reduces thermal losses. Additionally, few studies have examined various absorber designs in non-evacuated systems under non-uniform heat flux conditions, accounting for optical flux distribution and actual heat losses. Moreover, there are very few investigations in the literature that evaluate the thermo-hydraulic performance of various absorber geometries in non-evacuated and stationary operation, through both experimental and numerical validation.

In this regard, the present work tries to fill this gap by investigating a low-cost, small-scale, and non-evacuated stationary parabolic trough collector equipped with different absorber tube geometries, operating for domestic water heating applications. Unlike most of the published research, this study focuses on the absence of vacuum insulation, in favor of simplicity, price, and deployment convenience. Instead, it tries to enhance the collector performance by introducing novel tubular designs for the receiver unit as an innovative solution for future residential applications. The main objective is to compare various tubular receiver designs that accommodate the same (1 m) length of absorber zone (focal line). Also, exploring the role of the absorber geometries on the behavior of the surrounding air and forming the convective heat loss under non-uniform solar flux in the glass envelope is another point of novelty considered here. In this context, a coupled optical and CFD framework is used in conjunction with experimental data to conduct a thorough thermo-hydraulic assessment. Then, using the verified computational model, simple, helical, and sinusoidal receiver topologies are carefully compared, emphasizing the trade-offs between hydraulic penalties, exergy performance, and thermal efficiency under realistic working conditions.

2. Experimental description

The PTC system investigated in this study was manufactured, assembled, and tested experimentally at the National Engineering School of Gabes, Tunisia, in the Laboratory of Mechanical Modeling, Energy, and Materials (LM2EM), as detailed in Ref. [9]. Fig. 1 shows the complete experimental setup used to assess different receiver tube geometries under outdoor conditions. The prototype consists of a cylindro-parabolic reflector with an aperture width and axial length of 1 m each. The absorber area is 1 m long and is enclosed inside a glass envelope (outer diameter: 50 mm, inner diameter: 46 mm) to be protected from the surrounding environment. The studied absorbers were coated in a black matte finish to improve their ability to absorb sunlight. Moreover, the collector was fixed

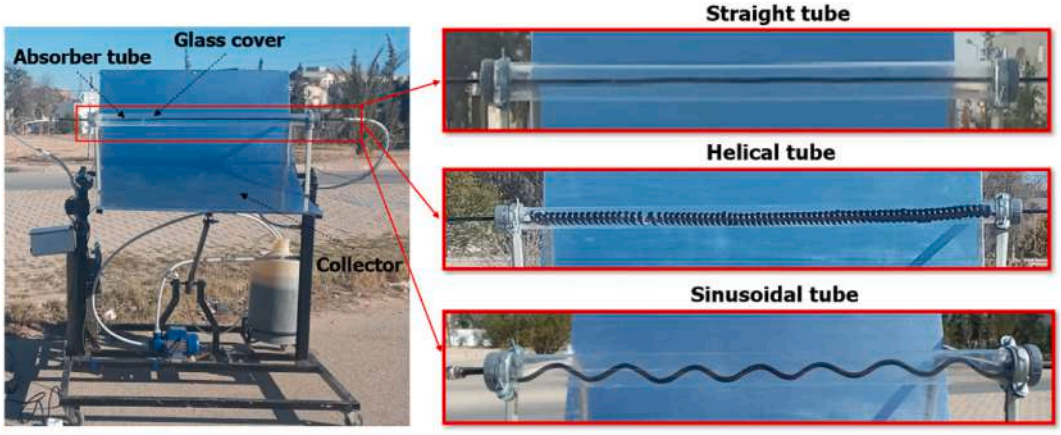

Fig. 1. Photograph of the experimental setup of PTC with different solar receivers.

to a metal support structure that permits angular modifications for daily adjustments.

Alongside the simple tube, three alternative geometries were developed to enhance heat transfer through the receiver unit, including a helical tube with 76 helical turns (R2), and two sinusoidal tubes with seven wave cycles: one in a plane perpendicular to gravity *g* (R3) and the other sinusoidal tube in a plane parallel to *g* (R4) to the collection axis. As a result, four different absorber configurations were examined in this study (Fig. 2). Also, in order to ensure uniformity across tests and enable direct performance comparisons, the absorber tubes for every arrangement had the same inner and outer diameters and were installed over the same reflector length (1 m). However, the actual tube lengths were influenced by the receiver geometry, resulting in 1, 6.6, and 1.1 m for simple absorber (R1), helical tube (R2), and sinusoidal configurations (R3 and R4), respectively. Table 1 provides a summary of the collector components as well as their geometrical characteristics.

Experiments were carried out on several consecutive days, trying to evaluate the performance of each tube geometry under a constant mass flow. Every tube was monitored during a full-day operation at two replications, and results were recorded at different time points. Ref. [9] include a detailed discussion on the experimental test procedures and result analyses. This study uses experimental boundary conditions to verify and validate the developed CFD models. Table 2 summarizes the experimental test conditions for

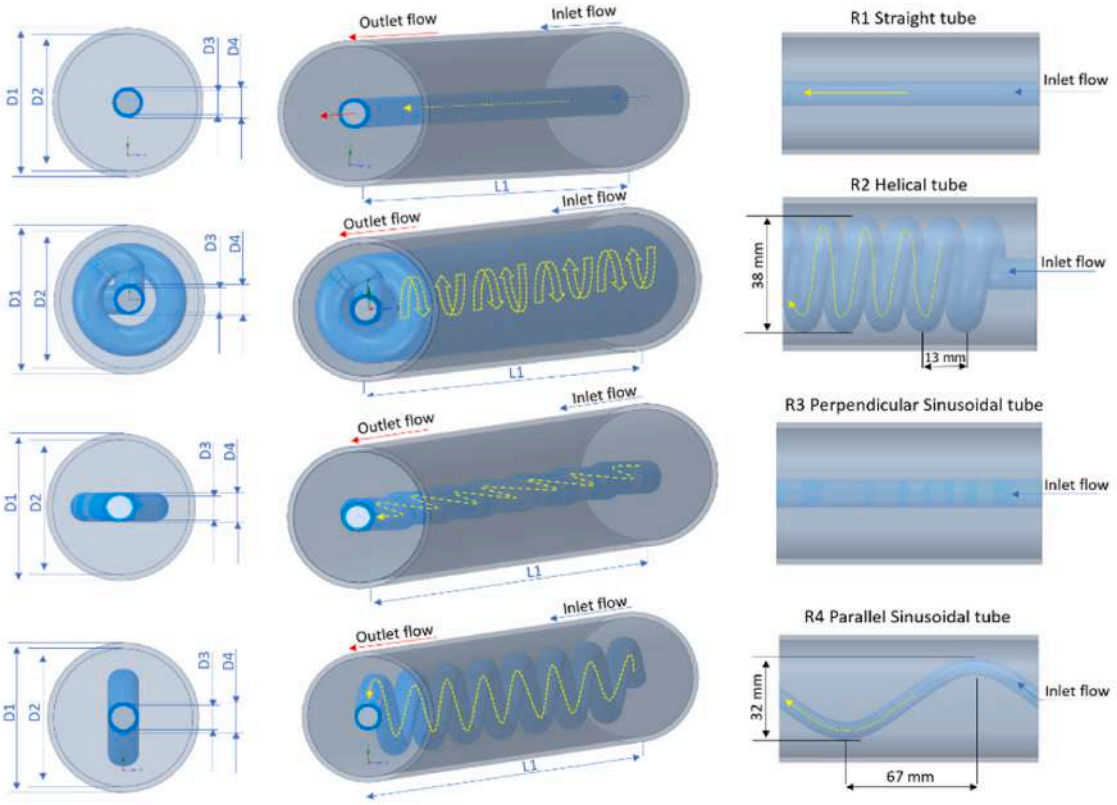

(a)

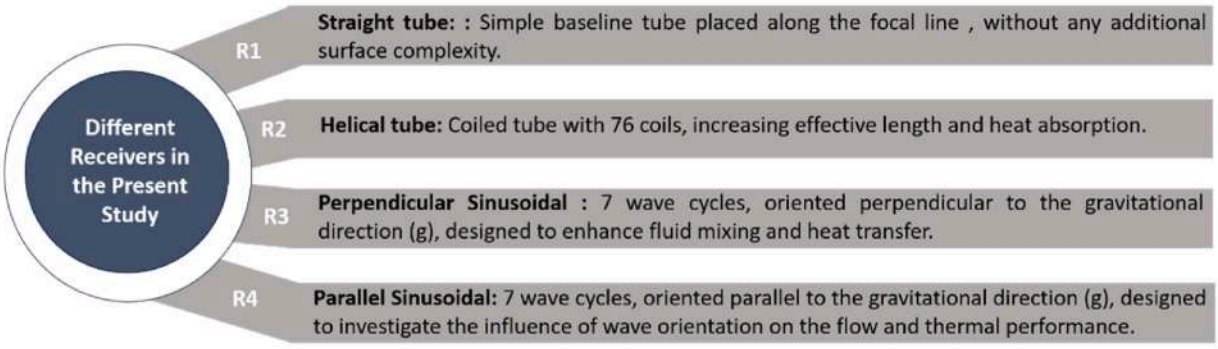

(b)

Fig. 2. (a) Different views of the studied receiver tubes, (b) design specifications of each receiver.

Table 1
Description of the receiver tubes.

Parameter	Symbol	Value (m)
Receiver axial length	L_1	1
Glass cover outer diameter	D_1	0.05
Glass cover inner diameter	D_2	0.046
Absorber tube outer diameter	D_3	0.01
Absorber tube inner diameter	D_4	0.008

the examined PTC with different tube configurations.

3. Numerical approach

A coupled optical-thermo-hydraulic process is developed to simulate the studied PTC collectors. This procedure entailed simulating the trajectory of solar radiation as it is focused onto the receiver tube after reflecting off the parabolic mirror. Fig. 3 shows every step of the simulation process, which combines a Monte Carlo Ray Tracing (MCRT) optical model and CFD simulations [34]. During this process, the PTC collector was designed in Tonatiuh software, respecting the optical and geometrical characteristics of the receiver and reflector and ray tracing is performed to achieve the flux distribution along the receiver [35]. In the next step, a User Defined Function (UDF) was created using optical results to define the thermal driver on the receiver component. This UDF was then integrated into the STAR-CCM + software to specify the non-uniform heat flux boundary condition on the absorber outer wall [36]. Achieving convergence on CFD simulations, with an iteration error of less than 10^{-5} for both hydraulic and thermal parameters, numerical data was extracted and post-processed for further investigations.

3.1. Optical analysis: Heat flux on the receivers

This methodology was applied to the simple tube, helical tube, and sinusoidal tube receiver configurations that were examined in this work. A distinct MCRT simulation was carried out for every shape using Tonatiuh, accounting for the particular orientation and spatial location of the absorber within the PTC system. Comparable methods for assessing intricate absorber geometries with MCRT tools have been documented in the literature [37]. The outcomes of heat flux distributions were exported separately and varied depending on the shape of the receiver. Optical investigations were carried out for an incident angle of 0, simulating solar noon on the testing days. Fig. 4 illustrates the four geometries modeled in optical simulations, displaying the ray tracing process for each design. The optical parameters utilized in the MCRT model were assumed constant for all receiver configurations. This assumption was made based on the fact that in a low-temperature (<80 °C) concentrating solar system, optical parameters remain nearly constant and unchanged, similar to Ref. [38]. A pillbox sun shape with a half-angle of 4.65 mrad was selected. The same optical assumptions were applied to all geometries to isolate the effect of receiver shape. The optical simulations demonstrated a significantly non-uniform heat flux profile over the absorber tube surface [39]. Flux analysis revealed that the area directly facing the parabolic mirror, where the reflected radiation is concentrated, absorbs the highest heat flux. While the upper segment of the tube receives only direct flux. This asymmetric heating directly affects the fluid working into the receivers and thermal behavior. These irregular heat flow patterns are in line with research in the literature, which indicates that the optical arrangement of the collector causes the absorber bottom side to receive the highest concentration [40]. Table 3 summarizes the optical results obtained through the MCRT method. As observed, the helical receiver (R2) absorbs the highest power due to a larger absorbing area and a wider cylindrical absorber area it provides. Comparing R1 and R3 receivers, it is shown that the sinusoidal absorber enhances optical behavior, expanding the receiving area along the horizontal plane parallel to the collector aperture. However, in the case of R4 geometry, the expansion in the parallel plane allows a fraction of reflected rays to escape before being absorbed by the receiver. As a result, R4 reflects the worst optical performance with minimum absorbed power.

Table 2
Summary of experimental parameters and DNI for PTC tests.

Tube designs	Test dates	T_{amb} (°C)	T_{in} (°C)	DNI (W/m^2)
R1	Day1(11/03/2023)	24-31	30-39	610-1040
	Day2 (14/03/2023)	25-30	27-39	600-1020
R2	Day1(11/04/2023)	21-25	28-38	540-980
	Day2 (13/04/2023)	22-32	33-37	450-1160
R3	Day1 (15/04/2023	22-28	30-34	300-950
	Day2 (26/04/2023)	23-26	30-34	330-780
R4	Day1 (27/04/2023	23-26	30-34	300-720
	Day2 (29/04/2023)	23-27	30-34	410-760

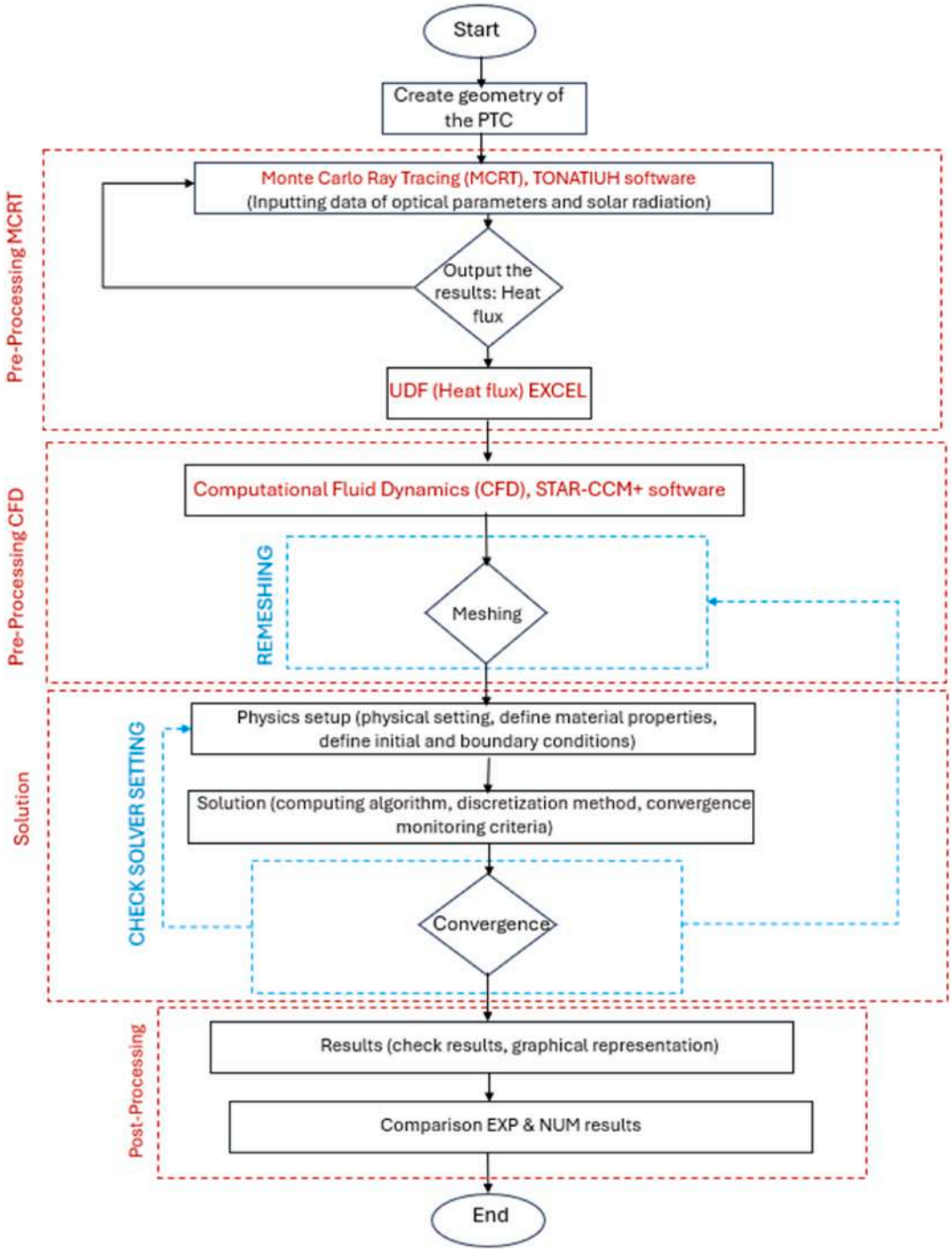

Fig. 3. Flowchart for MCRT and CFD analysis of PTC adopted in this work.

3.2. CFD simulation

In this study, a CFD model is developed based on the conditions extracted from the experiments, and under steady-state operating conditions. A three-dimensional computational domain was created for each receiver shape (R1, R2, R3, and R4 tubes) in order to meticulously model the heat transfer and fluid flow inside the PTC system. The physical domain includes a fluid region for water, a solid region for metallic pipe, another fluid region for air-filled annulus and another solid region for glass cover (Fig. 5). The fluid regime was set as laminar and a segregated flow temperature model was used for conjugate heat transfer analysis. Moreover, radiative

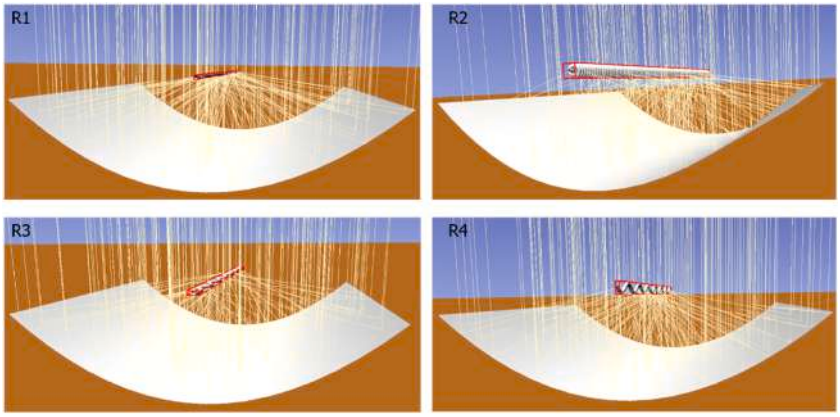

Fig. 4. Ray tracing process applied to the various PTC absorber geometries, using Tonatiuh software.

Table 3
Optical simulation results for an incident angle of 0 and $DNI = 1000$ W/m^2.

Tube designs	Incident power (W)	Absorbed power (W)
R1	1000	700
R2	1000	940
R3	1000	800
R4	1000	480

heat exchange between the absorber and glass envelope surfaces is simulated using the Surface-to-Surface (S2S) radiation model [23, 41]. This model is suitable for the vacuum or air-filled annular area between the absorber and glass tube in a PTC system. It should be mentioned that in order to define the absorber solid region as an opaque region, physical options were set as only external radiation exchange. However, the glass region was selected as both an internal and external radiation exchanging region to act as a transparent object [25]. The other numerical assumptions used in this study are listed below.

- Working fluid: a mass flow rate of 0.005 kg/s is specified for the fluid inlet, the inlet temperature was set as the experimental data for every receiver, the outlet face was adjusted as pressure outlet, and the flow is considered laminar.
- Air between the receiver and the glass envelope was simulated as a steady, laminar 3D flow, with natural convection and no-slip conditions at the walls.
- Absorber tube: a heat flux boundary condition was applied on the outer surface using a UDF obtained from MCRT analysis.
- Glass envelope: the physical options for the radiation model were specified as a transparent object, using both internal and external optical parameters.
- The solution domain contains four different regions, including the water (HTF), absorber tube, air, and glass envelope.
- Thermal losses were simulated by using the radiation model and applying a convective heat coefficient (h_w) of 10 W/m^{2}K.
- As this study considers the natural convection inside the glass envelope, the buoyancy effect was turned on during simulations.

Heat transport in a non-evacuated receiver is largely dependent on buoyancy-driven natural convection. As the ambient air is heated by the absorber tube, its temperature rises and its density falls, pushing the warmer air upward and generating circulation in the air gap. The gravitational term g describes this process, connecting buoyancy forces in the momentum equation to temperature-influenced density fluctuations. As a result, this density stratification has a significant impact on the temperature and velocity fields in the air domain, making buoyancy an important mechanism for heat transfer between the absorber surface and the glass envelope. Fig. 5 shows the applied boundary conditions for the different receiver tubes, and the simulations were predicated on the following factors. The various physical parameters of components examined in the PTC system are presented in Table 4.

3.3. Thermal modeling and data analysis

This section discusses the methodology used to model and analyze the thermal performance of the developed receivers. Therefore, in the first step, the useful thermal energy (Q_u) that the working fluid gains as it passes through the system is represented by Eq. (1) [42].

$$Q_u = \dot{m}\, C_p\, (T_{out} - T_{in}) \tag{1}$$

The available solar energy, represented by Q_s, is determined based on the characteristics of PTC, which can be estimated using Eq. (2) [43].

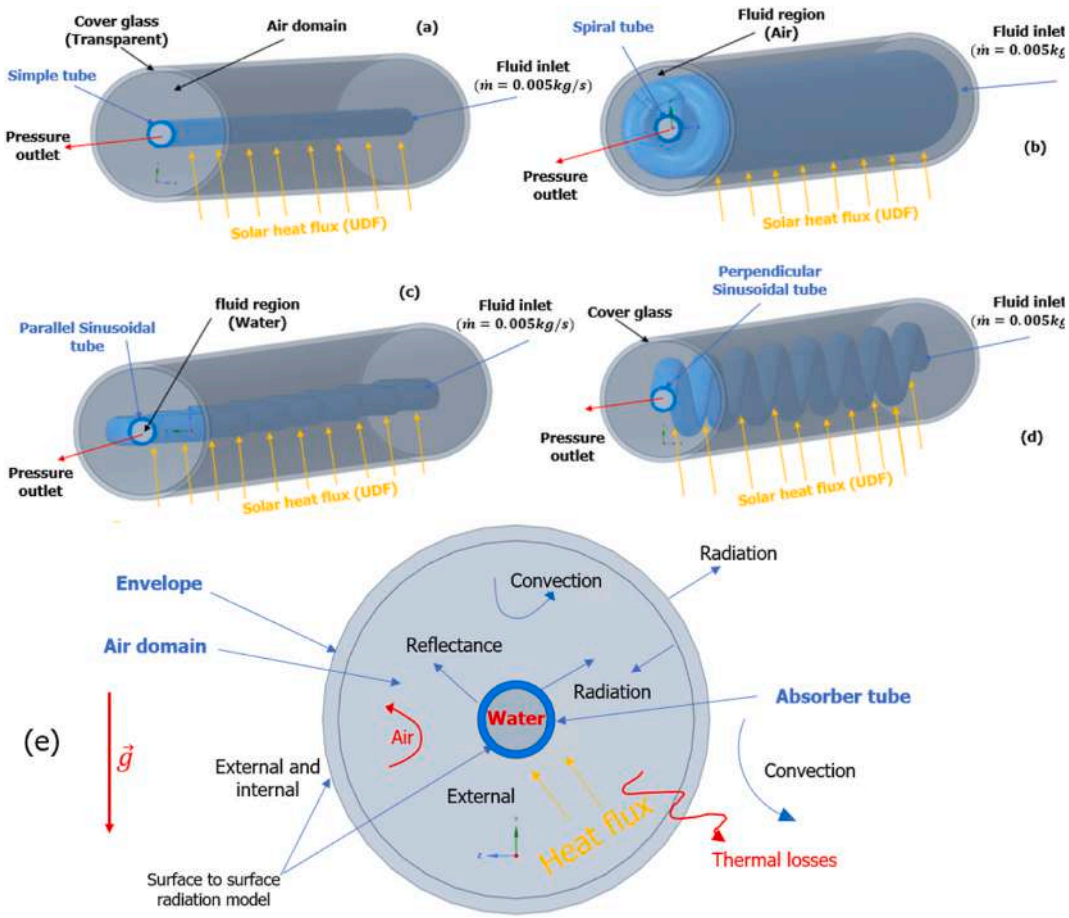

Fig. 5. Boundary conditions applied to the receiver tubes, (a) R1 (b) R2, (c) R3, (d) R4 tube, (e) the physical domain developed for the heat transfer between the receiver components.

Table 4
Material specifications for solid components and fluid domains.

Parameter	Material	Density (kg/m^3)	Specific Heat (J/kg.K)	Thermal Conductivity (W/m.K)	Temperature range (K)
Glass envelope	Glass	2230	850	1.1	-
Absorber tube	Copper	8027	500	20	-
Air region	Air	9E-06T^2-0.0094T + 3.17	0.0006T^2-0.3704T + 1064.3	-3E-08T^2+9E-05T + 0.001	288-393
Water region	Water	997.561	4181.72	0.62	-

$$Q_s = \eta_{opt}\, A_a\, DNI \tag{2}$$

The average optical efficiency (η_{opt}) used in simulations was derived directly from optical simulations, and an average value was used for assessing the operation at different times of the day. Although η_{opt} is a variable factor and depends on the hourly sun movement, this study tried to adopt an average value that represents the collector's performance during the entire day for the sake of simplicity and generality in the models. It should be noted that this parameter considers the collector optical properties, as well as tube absorptivity and glass transmissivity [44].

The ratio of the useful thermal energy delivered to the energy available from the sun is known as the PTC thermal efficiency, which can be determined by Eq. (3) [45].

$$\eta_{th} = \frac{Q_u}{Q_s} \tag{3}$$

Although thermal energy efficiency shows how well the system transforms solar radiation into heat energy that the working fluid can use, exergy efficiency expresses the quality of this energy and how effectively the system uses the source. Therefore, the exergy efficiency of the PTC (η_{ex}), which is the ratio of the exergy obtained by the collector to the exergy delivered by the incident solar

radiation, is the maximum usable work that may be obtained from the collector (Eq. (4)) [46].

$$\eta_{ex} = \frac{E_u}{E_s} \tag{4}$$

In this regard, the useful exergy output (E_u), reflecting the net amount of incoming and outgoing exergies, can be given as Eq. (5) [47].

$$E_u = Q_u - \dot{m}\, C_p\, T_{amb} \ln\left[\frac{T_{out}}{T_{in}}\right] - \frac{T_{amb}\ \dot{m}\ \Delta P}{T_{fm}\ \rho_{0fm}} \tag{5}$$

where the mean fluid temperature (T_{fm}) can be obtained as Eq. (6).

$$T_{fm} = \frac{T_{in} + T_{out}}{2} \tag{6}$$

while the exergy flow of incident solar irradiation (E_s) is computed by Eq. (7) [48].

$$E_s = w\, L_1 DNI \left(1 - \frac{4}{3}\left(\frac{T_{amb}}{T_s}\right) + \frac{1}{3}\left(\frac{T_{amb}}{T_s}\right)^4\right) \tag{7}$$

The sun's temperature (T_s) was assumed to be 5770 K, which is a typical value for the sun's outer layers [49].

In order to assess the heat transfer enhancement, measuring the Nusselt number under steady-state conditions is essential. For this purpose, the convective heat transfer coefficient (h) was computed through Q_u and the temperature difference between the fluid and receiver tube, using Eq. (8) [43].

$$h = \frac{Q_u}{\pi\, D_4\, L_a\left(T_{abs} - T_{fm}\right)} \tag{8}$$

As a result, the dimensionless Nusselt number (N_u), which represents the ratio of convective to conductive heat transport, was calculated by Eq. (9).

$$N_u = \frac{h\, D_4}{\lambda_{bf}} \tag{9}$$

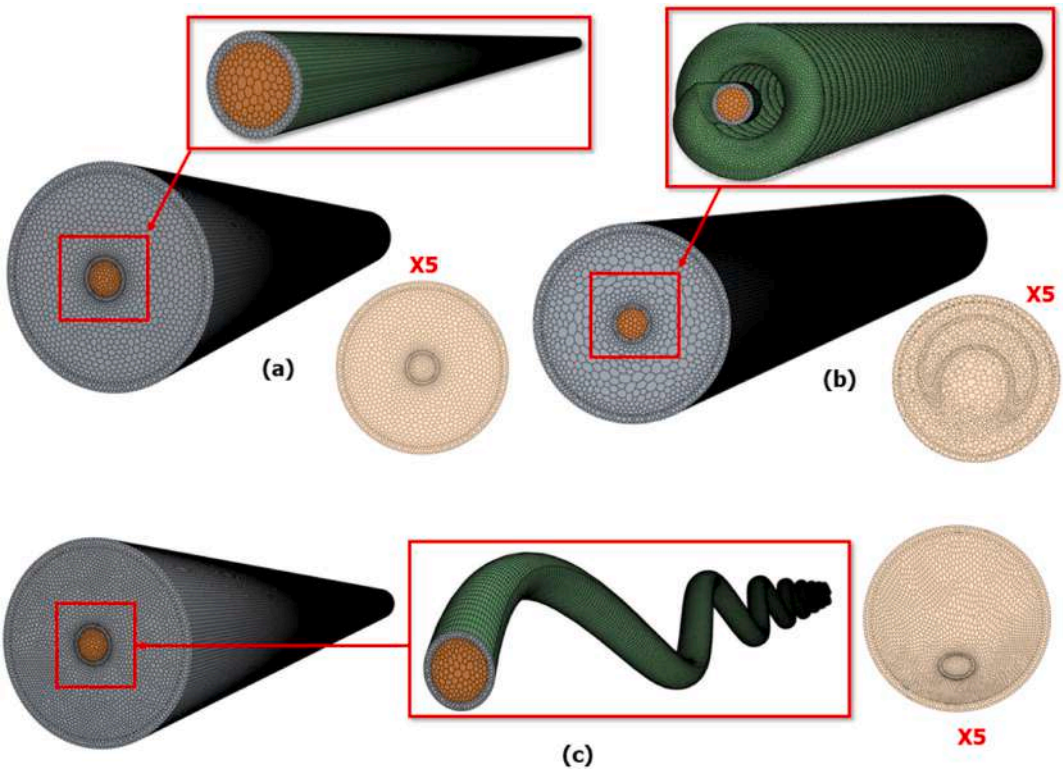

Fig. 6. Mesh networks developed in this study for various tube receivers: (a) R1, (b) R2, and (c) R3-R4.

The friction factor in the absorber tube is related to the pressure drop (ΔP) along the pipe. The description is determined by Eq. (10) [50].

$$f = \frac{2\,\Delta P\,D_4}{\rho_{0fm}\,V^2\,L_a} \tag{10}$$

where ΔP is determined as the difference between inlet and outlet pressures ($\Delta P = P_{in} - P_{out}$),
L_a is the actual absorber tube length, and V indicates the mean flow velocity.

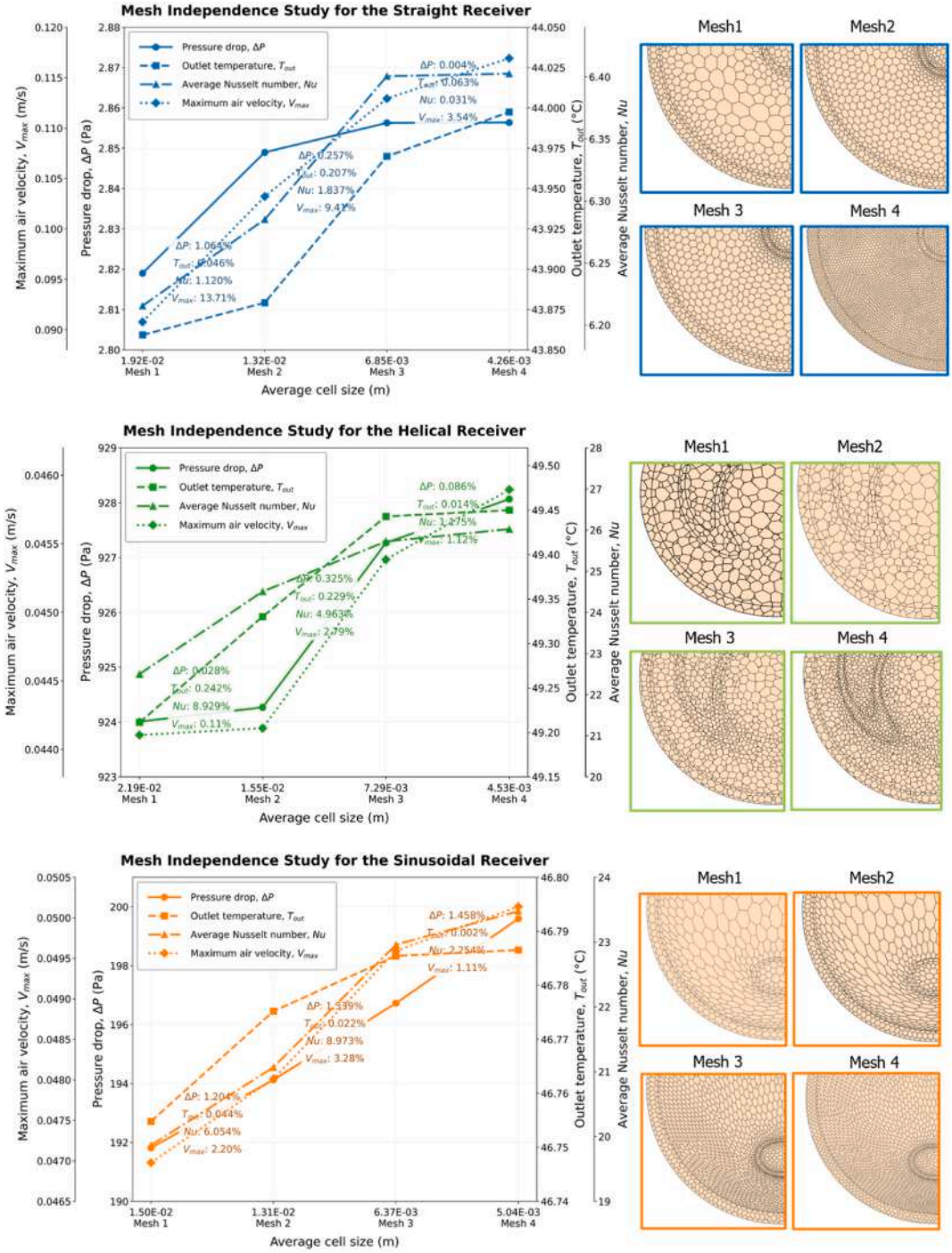

Fig. 7. Variation of ΔP, T_{out} , V_{max} and Nu with different mesh resolutions for the different tubes.

The overall efficiency (η_{ovr}), which evaluates the pumping power needed as the corresponding primary energy consumption, essentially determines the collector net usable heat generation, is computed by Eq. (11) [51].

$$\eta_{ovr} = \frac{Q_u - \frac{W_p}{\eta_{elec}}}{Q_s} \tag{11}$$

The average electrical efficiency of the grid is measured by electrical efficiency (η_{elec}), which was selected as 32.7% in this work. Furthermore, for the fluid flowing through the absorber tube, the pumping work demand (W_p) is computed by the following equation (Eq. (12)) [52].

$$W_p = \frac{\dot{m}\,\Delta P}{\rho_{0fm}} \tag{12}$$

3.4. Mesh study

Polygonal Mesher was used to provide the needed grid network, with some refinements in the area close to the solid-fluid interfaces, particularly around the curved surfaces of the absorber tubes. Verifying to what extent the numerical solution depends on the mesh size and that discretization errors have no effect on the findings was the aim of this mesh sensitivity investigation. Based on a trade-off between convergence stability, computational cost, and solution correctness, the ideal mesh can be chosen. The meshing topology for three receiver geometries: (a) simple tube, (b) spiral tube, and (c) sinusoidal tube, is shown in Fig. 6. In order to precisely capture heat transport and flow properties, both configurations (simple and sinusoidal tubes) use a structured mesh and are automated for the helical tube with very fine resolution in the fluid domain. In the zoomed-in views X5 (X = 50 cm), polyhedral cells are used to improve mesh quality and decrease numerical errors.

To verify the numerical accuracy of the solution, four meshes are assessed for each geometry, as shown in Fig. 7, and the pressure drop, outlet fluid temperature, maximum air velocity and Nusselt number were assessed as the convergence criterion. The average cell size was calculated as $\sqrt[3]{(V/N_{cell})}$, where N_{cell} is the number of cells, and V is the volume of all regions [53]. Fig. 7 illustrates how mesh convergence was processed for different shapes. A representative cross-sectional view of the mesh is included in each example. As seen, between Mesh 3 and Mesh 4, the mean variations in pressure drop are 0.004, 0.086, and 1.458% for the standard, helical, and sinusoidal receivers, respectively. The associated variations in outlet temperature were only 0.068, 0.014, and 0.002%, which indicates that further mesh refinement has no significant effect on the predicted outlet temperature. The average Nusselt number showed relative variances of 0.031, 1.175, and 2.254%. Maximum air velocity also provides a range of sensitivities, including 3.54, 1.12, and

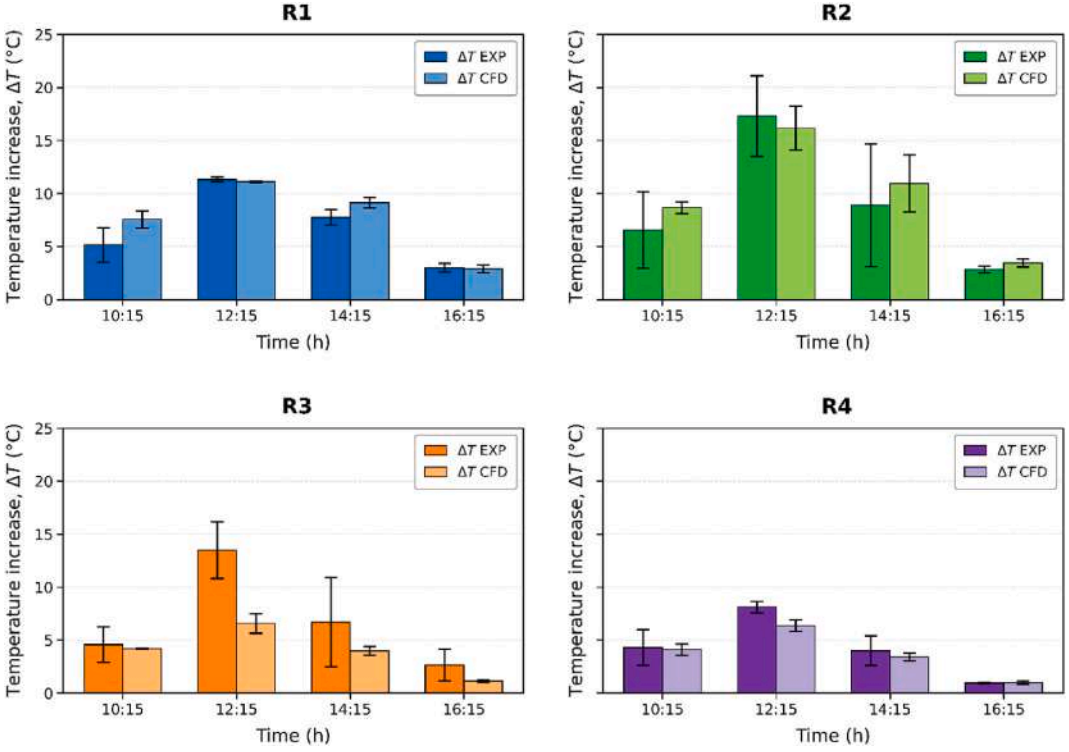

Fig. 8. Comparison of fluid temperature increase ($\Delta T = T_{out} - T_{in}$) for different receivers: (R1-R4).

1.11%, displaying a confidence level of 97% for the computed results in the annulus region. Given the relatively minor differences in the global thermo-hydraulic parameters, as well as the large increase in computational cost associated with the finest mesh, Mesh 3 was selected for all receiver configurations as the optimal balance of computational economy and numerical accuracy.

4. Validation

This section represents the validation process that is carried out to assess the accuracy of the developed numerical models, simulating the identical experimental conditions. In this regard, Fig. 8 presents the comparison between the fluid temperature data obtained by experimental measurements and numerical predictions through the four absorber configurations (R1–R4). Results are reported over the two consecutive days of measurements at different time points, and they correspond to the average temperature increase ($\Delta T = T_{out} - T_{in}$). The standard deviation is represented by the error bars, which show variability brought on by shifting ambient and solar conditions. The overall agreement seen between the CFD and experimental results lies in an acceptable range for all the cases studied. One important interpretation is how the average optical efficiency represents the hourly behavior of collector performance, which implies the highest accuracy (minimum difference) at 12:15 p.m., when the collector achieves its maximum performance. Moreover, the numerical forecasts display consistent patterns, even if larger standard deviation values indicate greater experimental error. This implies that the observed discrepancies are caused by experimental variations rather than modeling errors. Overall, the numerical model is deemed reliable for modeling the thermal performance of different receiver shapes in a PTC system.

5. Comparative numerical results

To fairly compare the thermal performance of each PTC receiver and adopt the most optimum design for DHW applications, this section analyses the CFD simulation carried out under similar boundary conditions. Therefore, a set of identical inputs, including $T_{in} = 30$ °C, $T_{amb} = 25$ °C, and $DNI = 1000$ W/m^2, is used for the analysis of four different receiver geometries.

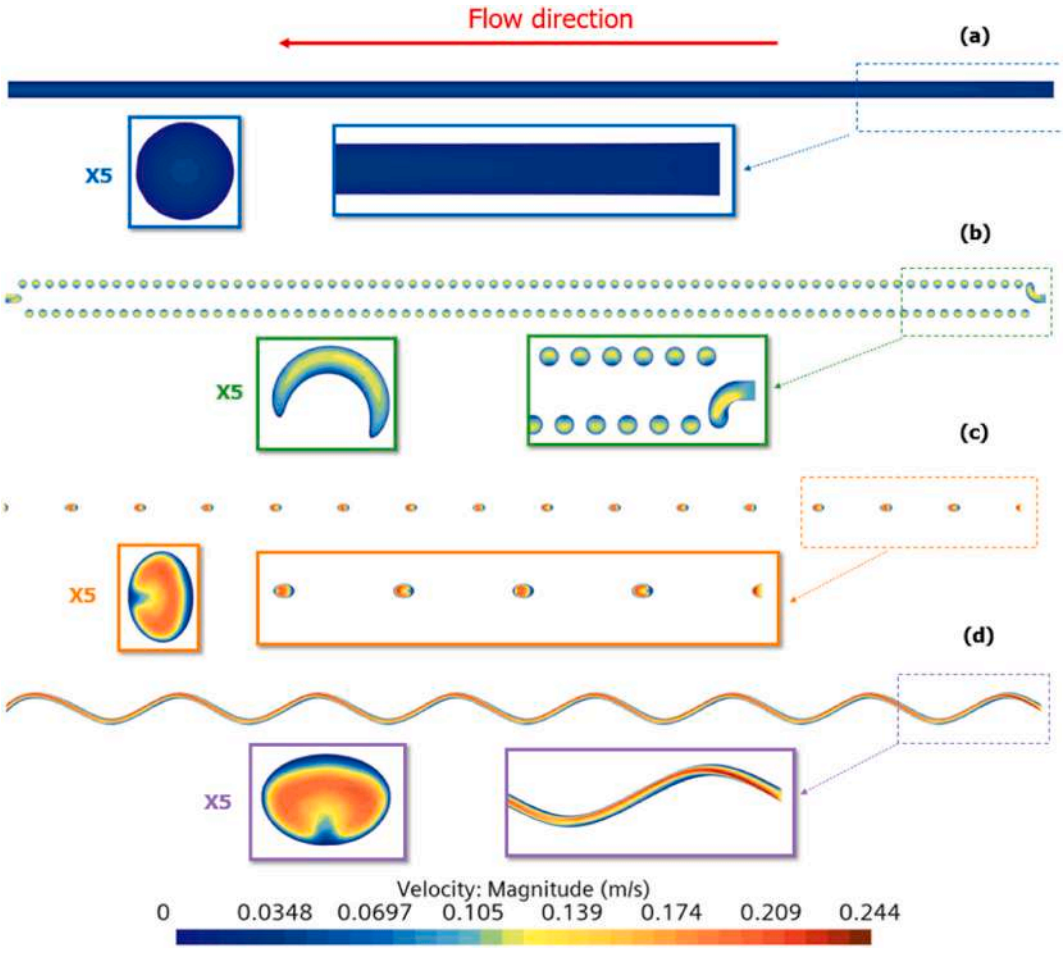

Fig. 9. Velocity distribution in the water domain for different receiver configurations; (a) R1, (b) R2, (c) R3, and (d) R4.

5.1. Hydraulic analysis

Fig. 9 presents the velocity map of water flow inside four different absorber tube designs. As expected, the centerline experiences the highest velocities, and the walls the lowest. This usual velocity pattern for the R1 shape is confirmed by the cross-sectional view in the YZ plane and the zoomed-in views X5. In the case of the R2 tube, the tube curvature would result in complex fluid flow, where centrifugal forces would push water toward the coil's outer wall, causing it to rotate around its axis. On the other hand, the sinusoidal shape curvature, R3, shows a distorted velocity profile throughout the axial sections, where the flow shifts toward one side due to the curvature of the sinusoidal geometry. Higher peak velocities than R1 result from complex flow patterns and improved mixing. R4 receiver exhibits considerably more pronounced flow distortion and mixing due to its sinusoidal course that is perpendicular to the collector. The velocity distribution seems more uniform, with higher magnitudes close to the walls and less distinct parabolic forms. This is a result of the wavy geometry and constant directional change, which increases fluid mixing. In comparison to the simple tube R1, the other tubes R2, R3, and R4 improve fluid agitation and velocity dispersion overall, which may lead to better heat transfer

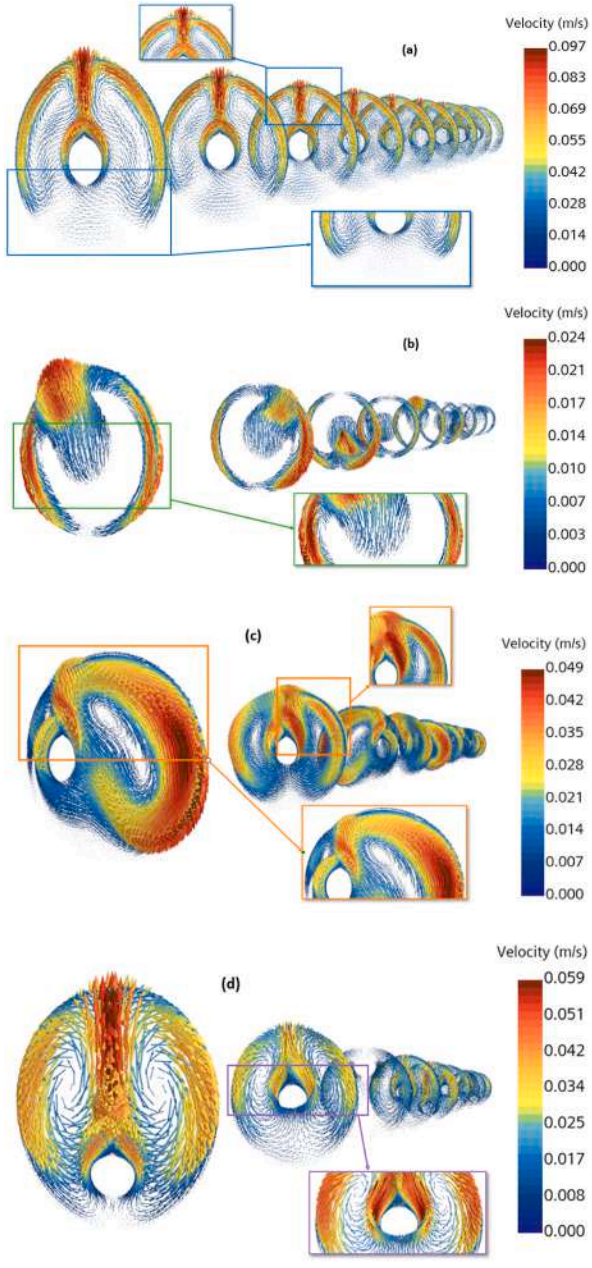

Fig. 10. Air velocity vector inside the annulus for different receivers; (a) R1, (b) R2, (c) R3, and (d) R4.

performance.

Fig. 10 depicts the velocity vector fields in the air domain around the four receiver configurations (a) R1, (b) R2, (c) R3, and (d) R4. In this process, the air buoyancy effect is the main flow driver, which promotes natural convection within the envelope region and varies depending on the absorber. The airflow in the case of R1 receiver (Fig. 10a) displays a comparatively symmetric pattern, and the air moves smoothly from the bottom to the top of the air domain, generating a stable upward flow as the simple tube heats uniformly. The air also moves from the bottom to the top in the R2 tube (Fig. 10b) as well, but the helical shape causes swirling patterns, which reduce the air velocity more than R1 in the annular area. R3 shape (Fig. 10c) creates alternating vortex patterns that affect heat transfer from the tube surface by regularly disturbing the air throughout the tube length. As a result, each wave crest and dip has different active air recirculation zones. The sinusoidal tube perpendicular orientation causes R4 (Fig. 10d) to exhibit even more intricate behavior than R3. Also, the air movements show a similar pattern as R1 with two symmetrical loops, while the sinusoidal shape enables disrupting these loops in the longitudinal direction, leading to slower air movements than R1. Among the proposed geometries, R2 enables the minimum air velocity inside the annulus region, promoting lower heat convection loss in this design. Moreover, considering the sinusoidal layouts, R3 mitigates the air recirculation in the annulus region by disturbing the two loops usually formed on the two sides of the absorber (10a). However, R4 allows the recirculation of air in the two identical loops similar to R1, bringing higher maximum air velocity than R3.

Table 5 compares the hydraulic performance of the different receiver designs and shows a strong relationship between flow resistance and tube shape. The modest pressure drop of 2.84 Pa is produced by the baseline R1 tube. The R2 tube, on the other hand, showed the greatest hydraulic resistance, with a pressure drop of 927.26 Pa, which is about 326 times higher than the baseline. Complex fluid flow that improves fluid mixing at the expense of high pumping power is the main cause of this abrupt increase. With the parallel orientation (R4) exhibiting somewhat higher resistance (205.98 Pa) than the perpendicular orientation (R3) (196.72 Pa), the geometries (R3 and R4) provide a more moderate rise in pressure drop.

5.2. Thermal analysis

The thermal performance of tube geometry is characterized by the fluid temperature increase at the outlet, shown in Fig. 11. The helical tube (R2) exhibits the most uniform temperature profile, demonstrating a significant improvement in heat transmission brought about by the extended heat transfer surface and better fluid mixing through the helical design. The simple tube (R1) shows a large radial temperature gradient, with heat concentrated near the walls and a cold core, indicating poor fluid mixing. The sinusoidal designs (R3 and R4) show medium mixing; the perpendicular orientation (R3) yields a more consistent profile, with higher temperatures, than its parallel counterpart (R4). This demonstrates that by disrupting the thermal boundary layer, geometric changes significantly improve the collector's heat transfer efficiency. The computed average outlet temperatures revealed that R2 provides the maximum level of 50 °C, which suggests a 14% improvement compared to the R1 case. R3, with a 7% increase over R1, ranks as the second optimum case for providing hot water among the proposed cases. While R4, with an outlet temperature of 40 °C lies below the levels produced by R1.

The evolution of the temperature increase within the various receiver configurations is shown in Fig. 12. R1 shows the largest and relatively sharp temperature increase with an average value of 30 K. The air temperature profile also suggests the direction of convection heat loss toward the upper section of the glass envelope, where the temperature rise is more dominant. R2 exhibits a modest temperature rise along the whole receiver length, reaching an average value of 10 K. The lower solid surface highlights the mitigated thermal losses, which is also evident in the rise of air temperature surrounding the helical tube. However, sinusoidal R3 reflects an increased temperature rise, with a value of 15 K on the absorber surface, indicating stronger thermal losses compared to R2. The lowest temperature rise refers to R4 with 9 K, which shows how geometry orientation can affect solar absorption and consequently thermal losses within the receiver area.

5.3. Evaluation of receiver efficiencies

The thermal and exergy efficiencies for each receiver configuration (R1-R4) are shown in Fig. 13. The findings clearly demonstrate that the alternative tube designs could improve the thermal performance of simplified PTC systems in terms of thermal energy efficiency. Where the maximum of 40% is obtained for the R2 configuration, reflecting more than a 38% improvement compared to the simple design. R3 also enhances thermal efficiency by 20%, providing the effects of improved fluid mixing, which was observed by the ΔT contours, encouraging more efficient heat transfer from the receiver wall to the working fluid. However, in the case of R4, the thermal efficiency decreases compared to the R1 receiver, which is attributed to its optical behaviour and the lower thermal power that

Table 5
Pressure drops for the different configurations of the solar receiver.

Configuration	ΔP (Pa)
R1	2.84
R2	927.26
R3	196.72
R4	205.98

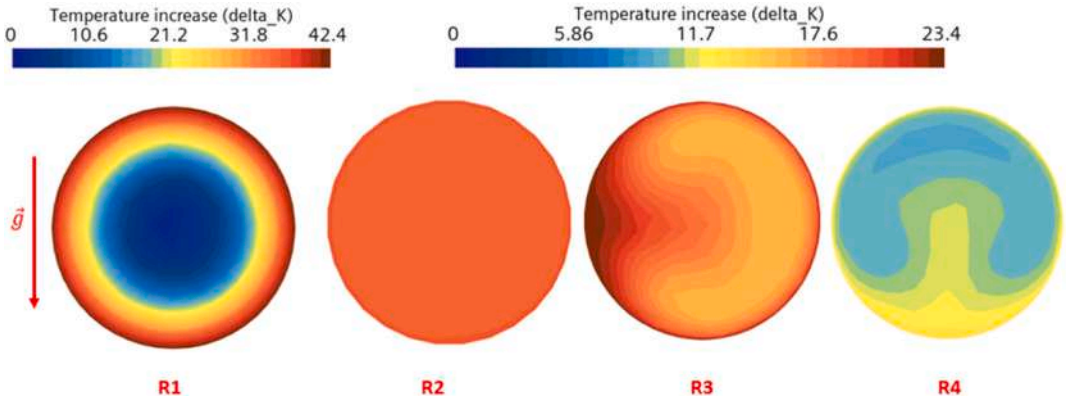

Fig. 11. Cross-sectional ΔT contours for configuration (R1-R4) at the receiver outlet.

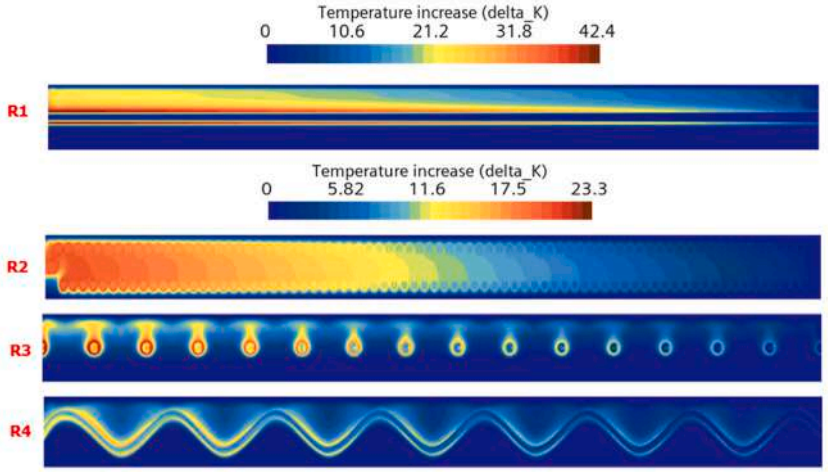

Fig. 12. Temperature increases in the YZ plane of the different receiver configurations: (R1-R4) (Flow direction: right to left).

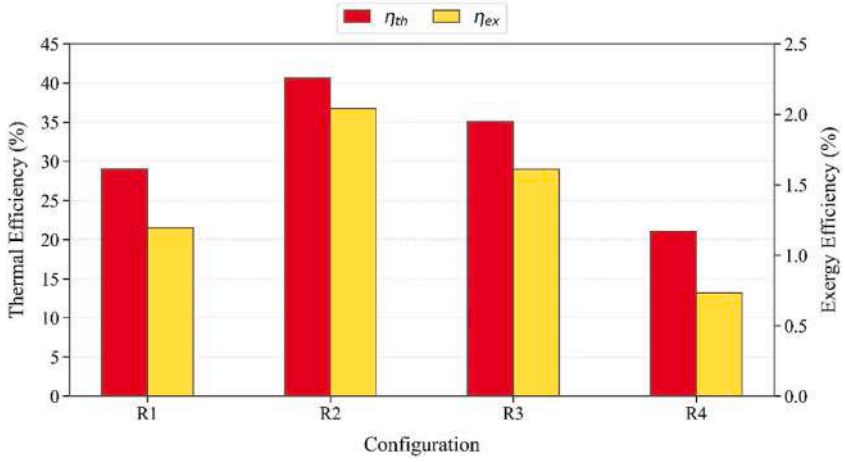

Fig. 13. Thermal and exergy efficiency for the various receiver configurations.

can be achieved compared to the R3 geometry (see Table 3). If compared with literature values for small-scale PTC, the thermal efficiencies reported in this study outweigh those of peer designs with 16.2% [54], 11.2% [55], and 4% [56]. Considering the exergy efficiency, the only tube design showing lower performance than the simple tube is R4. This can be attributed to the cooler surface

temperature compared to R3 and higher flow resistance than R1, which intensifies exergy destruction in R4. However, R2, with the hottest surface temperature and the lowest temperature difference from the sun, provides the maximum exergy efficiency of 2%. It should be noted that the levels of exergy efficiency obtained in this study are a common range in domestic solar water heating systems due to low-temperature operating conditions, which inherently have limited exergy content, as also reported by Ref. [33]. The findings demonstrate the helical absorber's ability to improve energy conversion efficiency and heat transmission, making it the best design among the four studied.

Fig. 14 depicts the thermo-hydraulic performance of four receiver configurations, with emphasis on the average *Nu*, *f*, and η_{ovr}. As shown in Fig. 14a, the R2 tube has the highest *Nu* (~30), indicating a significant increase in convective heat transfer when compared to the R1 tube (6.28). The sinusoidal receivers (R3 and R4) show *Nu* values of 25 and 24, respectively, reflecting their ability to increase the heat transfer compared to the R1 tube. However, R4 faces increased hydraulic resistance, having the highest *f* (0.3) compared to R1 with the lowest (0.005). While the R2 receiver poses moderate *f* with 0.22, showing lower values than sinusoidal receivers. Fig. 14b compares the η_{ovr} for various receiver models and shows the combined effects of thermal enhancement and pumping powers. In this context, the R2 receiver reaches the maximum value of η_{ovr} as 40%, suggesting an optimal thermo-hydraulic performance. The second optimum case is the sinusoidal receiver R3, which displays a higher overall efficiency than the R1 model, demonstrating that its higher pumping power can be justified by its higher thermal efficiency. However, the R4 receiver becomes the worst case as it requires high pumping power but provides low thermal efficiency. As a result, among those tested, the helical receiver was selected as the optimum case and is analyzed further in Section 6 under more testing conditions.

6. Performance analysis of the optimum case

This section focuses only on the optimum case (R2) selected in Section 5, providing further insights into its performance compared to the simple case. For this purpose, broader working conditions with different levels of water inlet temperature (30, 40, 50, and 60 °C) and mass flow rates (0.005, 0.0075, 0.01, and 0.0125 kg/s) are analyzed in terms of performance criteria. In this context, Fig. 15 displays the velocity vector fields in the annular air gap between the glass cover and the absorber tube at the receiver midplane cross-section (X5 = 50 cm) for input temperatures ranging from 30 °C to 60 °C. Results indicate that increasing the water inlet temperature accelerates the air movements in the annulus, suggesting higher thermal losses from the absorbers. Moreover, comparing the two designs, R1 shows more concentrated and powerful natural convection currents, which improve heat transmission from the absorber to the air gap and raise thermal losses as a result. On the other hand, R2 occupies a larger volume inside the annulus, which weakens air loop formations, restricting the strength of buoyancy-driven circulation. This implies that the convection heat loss from the absorber to the glass region is mitigated. Therefore, it further demonstrates that the altered flow structure brought about by the helical geometry will enhance the receiver thermal behaviour by reducing heat losses to the surroundings and encouraging more efficient heat transfer to the working fluid.

More performance criteria such as *Nu* and *f* are discussed in Fig. 16, analyzing their results as a function of different inlet temperatures and water mass flow rates. Fig. 16a illustrates how *Nu* and *f* change with inlet temperature. Both variants exhibit a slight decrease as the inlet temperature increases. But compared to R1, R2 has significantly higher *Nu* (more than 4.6 times), indicating improved convective heat transfer between the absorber wall and the working fluid. The better heat transfer performance of the helical tube is mainly due to the complex flow structures and increased fluid mixing caused by the helical design. Overall, the helical absorber (R2) retains significantly better thermal and heat transfer performance than the traditional absorber across the studied temperature range and can be a perfect candidate for adoption in DHW production systems. On the other hand, *f* remains almost constant as the input temperature increases for both receiver configurations, demonstrating that the hydraulic resistance is mostly determined by the receiver shape rather than the operating temperature. The helical receiver has a significantly larger *f* than the straight receiver (~47 times) due to the longer helical flow path and continuous curvature, which increase flow resistance and pressure losses. Fig. 16b depicts the effects of various mass flow rates and T_{in} = 30 °C on *Nu* and *f*, representing that *Nu* grows and *f* declines with a rise in $\dot{m}$. Comparing the two geometries demonstrates that increasing the $\dot{m}$, the improvement effects on *Nu* become more dominant in R2 (by 60%), rising from 0.005 to 0.0125 kg/s, while this growth is 33% in the R1 case. This implies that the complexity of flow in the helical absorber increases with higher *Re*, leading to higher heat transfer rates. From another point, *f* decreases more slowly (30%) in R2 with a rise in $\dot{m}$, which is a direct result of flow curvatures in the helical tube, and makes *f* less sensitive to $\dot{m}$ than the simple tube.

Fig. 17a displays the thermal efficiency variation for the R1 and R2 absorber topologies with respect to the temperature difference between the water inlet and ambient divided by the solar radiation, (T_{in}-T_{amb})/DNI. As the collector heats up, both receivers display a decreasing thermal efficiency due to an increase in convective and radiative heat losses. However, the efficiency value of the R2 design ranges from 41% to 37% while R1 fluctuates between 29% and 26%. Thus, the R2 receiver guarantees enhanced performance over the conventional R1 receiver at all inlet temperatures. Fig. 17b illustrates the overall efficiency as a function of inlet temperature, comparing the R1 and R2 receivers. This comparison highlights the balance between thermal performance enhancement and hydraulic losses in the two receiver designs. As seen, the effect of water inlet temperature is similar to that of thermal efficiency, resulting in lower overall efficiency as T_{in} grows. Moreover, the nearly identical values between thermal and overall efficiency refer to the negligible effects of pressure drop at the studied operating conditions. Therefore, the performance superiority of R2 over R1 can be confirmed considering both effects of heat transfer enhancement and pressure losses. Fig. 17c depicts a positive effect of increasing the water flow rate on the overall efficiency of the two receivers. The reason can be attributed to the fact that increasing $\dot{m}$ generally improves thermal performance more than it increases the hydraulic penalty. As a result, a maximum overall efficiency of 41% was achieved by R2 at $\dot{m}$ = 0.0125 kg/s, which is a 38.6% improvement over R1. The better heat transfer performance of the helical tube is

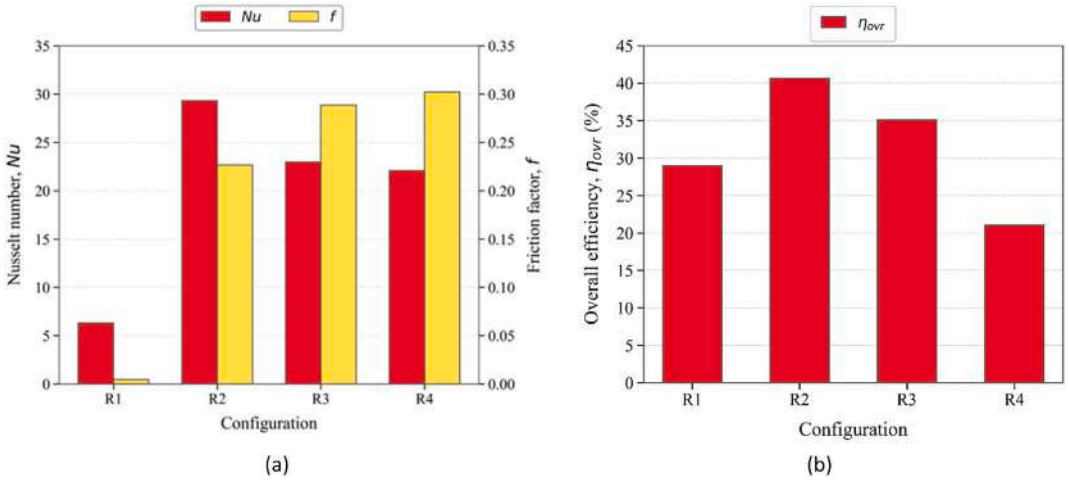

Fig. 14. (a) Comparison of average Nusselt number and friction factor and (b) variation of overall efficiency for different receiver configurations.

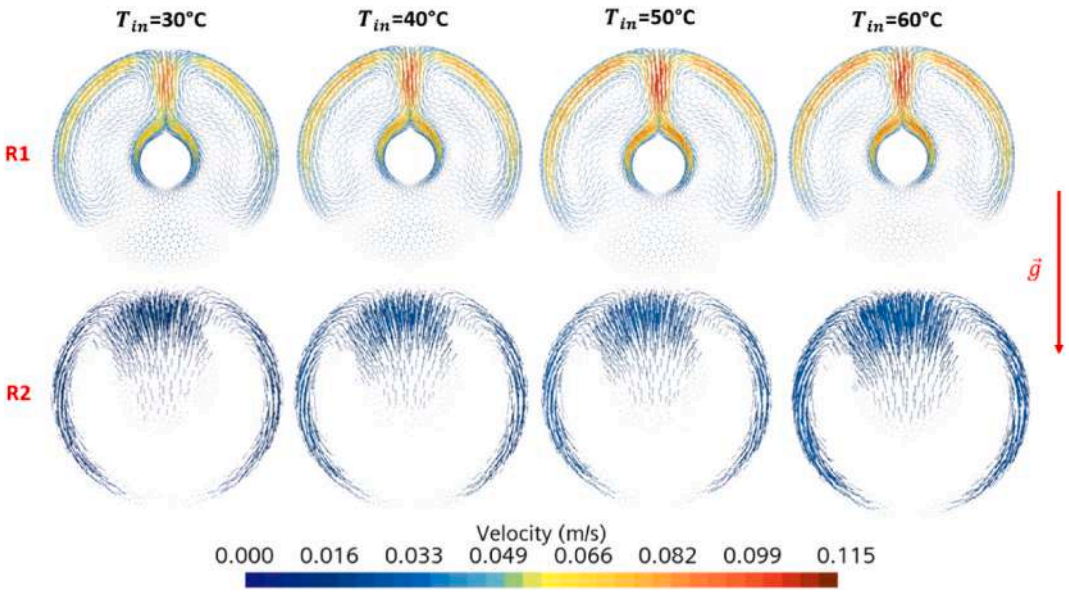

Fig. 15. Cross-sectional (midplane) air velocity vector for various tube R1 and R2 with different inlet water temperatures (30-60 °C).

a product of optical, thermal and hydraulic characteristics of the tube. Overall, the helical absorber (R2) retains significantly better thermal and heat transfer performance than the traditional absorber across the studied temperature range and can be a perfect candidate for adoption in DHW production systems.

7. Conclusions

This work presented an integrated experimental and numerical investigation of a small-scale PTC specifically designed for domestic water heating applications. The study focused on a low-cost, non-evacuated receiver configuration, aiming to propose a new solution for future solar-based water heaters. Four different absorber tube geometries: simple tube, a helical tube, and sinusoidal tubes with parallel and perpendicular orientations, were analyzed to assess their thermo-hydraulic performance under realistic outdoor operating conditions. A coupled optical–thermal numerical framework was developed by integrating MCRT simulations with 3D CFD modeling. The numerical results were validated against experimental measurements obtained from a prototype system, which displayed good agreement. This confirms the reliability of the proposed modeling approach for predicting the thermal behavior of non-evacuated PTC systems with complex absorber geometries. The following points represent a summary of the main outcomes of the present research.

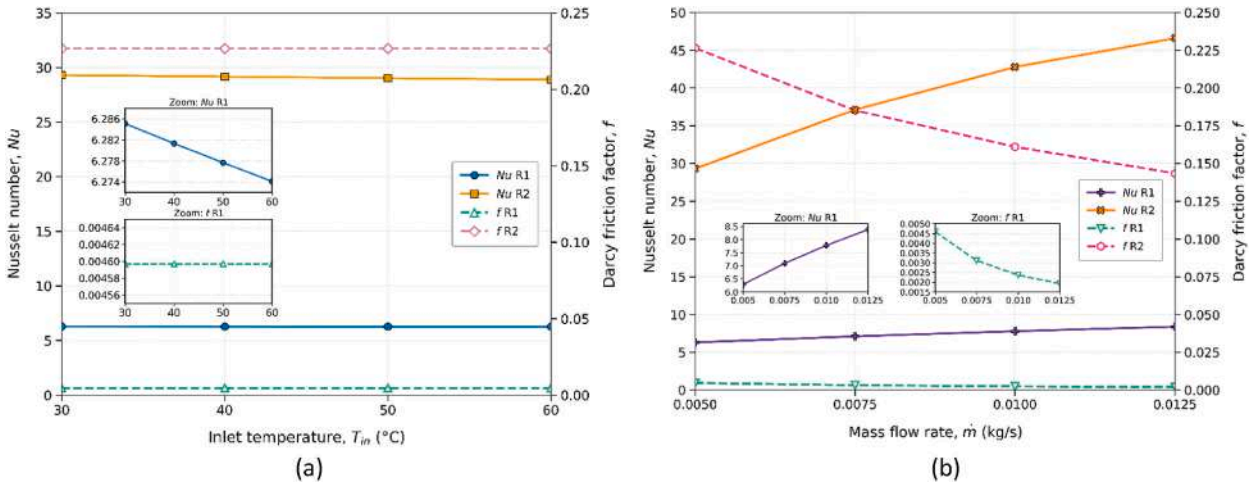

Fig. 16. Variation of *Nu* and *f* obtained as a function of various (a) inlet temperature and (b) water mass flow rate with $T_{in} = 30$ °C.

- Altering the absorber tube's geometry is a useful technique for improving non-evacuated stationary PTC performance. The combined effects of changes in optical, thermal and fluidic characteristics suggest increased internal heat flow in comparison to the traditional tube.
- The analysis emphasizes the importance of natural convection in non-evacuated receivers, pointing out that convective heat losses driven by absorber design are a result of the absence of vacuum insulation. In order to improve heat transfer along the tube, various shapes, such R2 and R3, create different air circulation patterns. R2 produces swirling patterns, while R3 produces alternating vortex patterns. Despite having symmetrical loops like R1, the R4 with a sinusoidal topology causes these loops to be disrupted longitudinally, which reduces air circulation.
- The orientation of the sinusoidal absorber was found to influence system behavior, with the perpendicular configuration showing an enhanced thermal performance compared to the parallel arrangement.
- The helical receiver had the greatest average *Nu* (~30), exceeding the simple case (6.3) and sinusoidal receiver configurations (23 and 22), indicating a significant improvement in convective heat transmission. However, these improvements were obtained with the penalty in pumping power, where the maximum *f* was determined by the R4 tube as 0.3.
- The thermal efficiency of up to 40%, achieved by R2, demonstrated that the stationary non-evacuated PTCs can operate with performance identical to stationary evacuated PTCs, as reported in Ref. [57]. This clearly highlights the effectiveness of changing absorber geometry in compensating for thermal losses associated with non-evacuated conditions, proposing a cheaper and simpler solution.
- Even though the helical receiver had the highest pressure drop due to the longer and curved flow path, the significant increase in convective heat transfer exceeded the corresponding hydraulic penalty, which resulted in a 38.6% higher overall efficiency than the conventional tube.

Although helical tubes may increase fabrication costs due to additional forming operations, mass production through automated coil-forming techniques could reduce these additional costs. Moreover, the compact design of a helical receiver offers fewer joints compared with multiple simple tubes connected for an equivalent length, which can reduce potential leakage points. However, the curved geometry may make the cleaning process more challenging, especially in regions where high mineral scaling is highly probable.

Future work will focus on further reducing convective heat losses within the annulus region and exploring additional passive enhancement strategies to improve overall system performance. Optimization of the geometric parameters, such as the helical tube pitch and tube diameter, should be considered in future work. It should be noted that performance enhancements achieved through the implementation of different receiver geometries in this study were obtained as a combined effect of optical, thermal and hydraulic characteristics. Future work should therefore consider a more controlled comparison with equivalent heat transfer area or tube length to isolate the effects of secondary flow and geometric enhancement. System-level analyses are also required to scale up the results of this study for deployment with residential home applications and assess their performance under annual operations.

CRediT authorship contribution statement

Jihen Mahdhi: Writing – original draft, Visualization, Software, Investigation, Data curation. **Hossein Ebadi:** Writing – original draft, Supervision, Software, Methodology, Data curation. **Abdallah Bouabidi:** Writing – review & editing, Resources, Project administration, Methodology, Conceptualization. **Ridha Ennetta:** Writing – review & editing, Supervision, Project administration, Methodology, Conceptualization. **Laura Savoldi:** Writing – review & editing, Validation, Supervision, Resources, Methodology, Conceptualization.

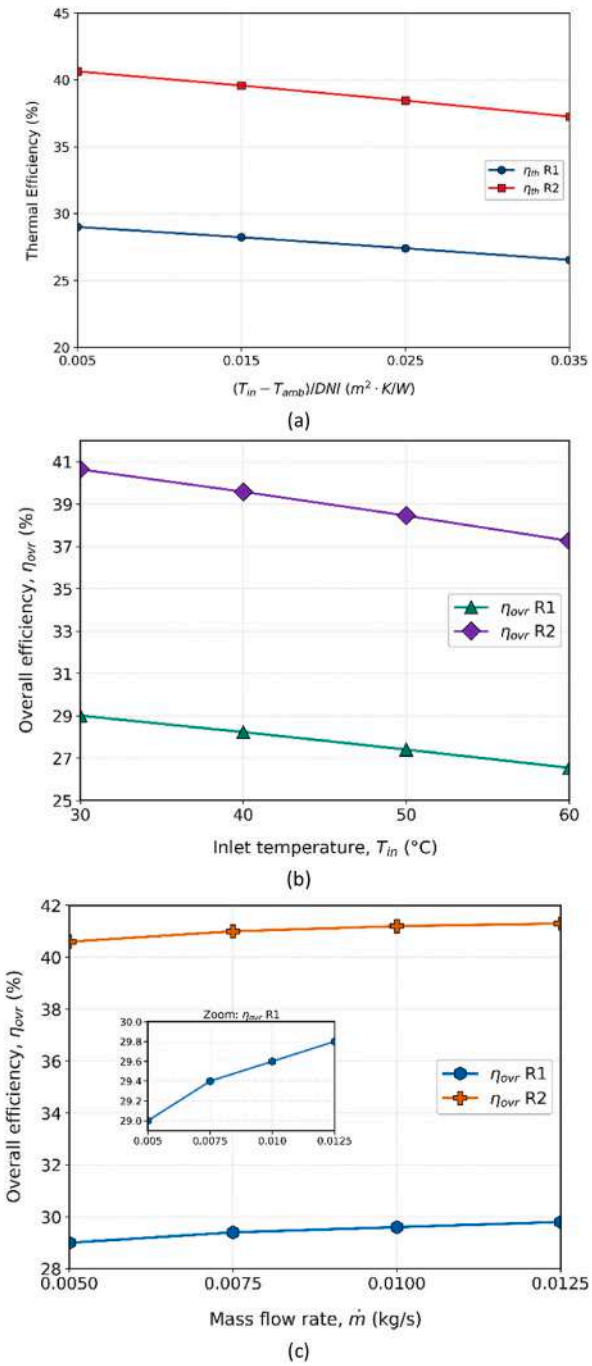

Fig. 17. Performance evaluations in terms of (a) thermal efficiency as well as overall efficiency as a function of (b) different inlet temperatures, and (c) various mass flow rates with $T_{in} = 30$ °C for R1 and R2 absorbers.

Declaration of competing interest

The authors declare that they have no known competing financial interests or personal relationships that could have appeared to influence the work reported in this paper.

Acknowledgment

We acknowledge the use of the computational resources provided by hpc@polito, which is a project of Academic Computing within

the Department of Control and Computer Engineering at the Politecnico di Torino (http://hpc.polito.it).

Nomenclature

Abbreviations	
CFD	Computational Fluid Dynamics
DHW	Domestic Hot Water
EXP	Experimental
HTF	Heat Transfer Fluid
MCRT	Monte Carlo Ray Tracing
PTC	Parabolic Trough Collectors
R1	Straight tube
R2	Helical tube
R3	Sinusoidal tube - perpendicular orientation
R4	Sinusoidal tube - parallel orientation
S2S	Surface to surface
UDF	User-Defined Function
Symbols	
A_a	Aperture area (m^2)
C_p	Specific heat (J/kgK)
D_1	Glass cover outer diameter (m)
D_2	Glass cover inner diameter (m)
D_3	Absorber tube outer diameter (m)
D_4	Absorber tube inner diameter (m)
DNI	Direct normal irradiance (W/m^2)
E_u	Useful exergy (W)
E_s	Solar exergy (W)
f	Friction factor (−)
g	Gravity acceleration (9. 81 m/s^2)
h	Heat transfer coefficient (W/m^2K)
L_1	Receiver axial length (m)
L_a	Actual absorber tube flow length (m)
$\dot{m}$	Mass flow rate (kg/s)
N_{cell}	Number of cells (−)
Nu	Nusselt number (−)
P	Pressure (Pa)
Q_u	Useful thermal energy (W)
Q_s	Available solar energy (W)
T	Temperature (K)
U	Total volume (m^3)
V	Velocity (m/s)
w	Collector width (m)
W_p	Pumping work demand (W)
Greek symbols	
ρ_0	Density (kg/m^3)
η	Efficiency (%)
ΔP	Pressure drop (Pa)
ΔT	Temperature increase (K)
λ_{bf}	Thermal conductivity of the base fluid (W/mK)
Subscripts	
abs	Tube absorber
amb	Ambient
elec	Electrical
ex	Exergy
fm	Fluid at mean temperature
in	Inlet
max	Maximum
opt	Optical
out	Outlet
ovr	Overall
s	Sun
th	Thermal
w	wind

Data availability

Data will be made available on request.

References

[1] L. Si, X. Zhou, H. Hou, Z. Zhou, K. Zhuang, Q. Liu, H. Zhang, A physically constrained hybrid modeling framework for real-time simulation of parabolic trough solar field in CSP plants, Appl. Therm. Eng. 289 (2026) 129730, https://doi.org/10.1016/j.applthermaleng.2026.129730.

[2] D. Leiria, H. Johra, A. Marszal-Pomianowska, M.Z. Pomianowski, A methodology to estimate space heating and domestic hot water energy demand profile in residential buildings from low-resolution heat meter data, Energy 263 (2023) 125705, https://doi.org/10.1016/j.energy.2022.125705.

[3] M.J.N. Oliveira Panão, M.V.L. Figueira, Decarbonizing residential water heating: pathways to cost-competitive energy solutions in the European context, Energy Build. 347 (2025) 116269, https://doi.org/10.1016/j.enbuild.2025.116269.

[4] O. Jafarli, Decarbonizing residential water heaters through solar energy: Long-term energy and emission impacts in Azerbaijan, Next Energy 11 (2026) 100581, https://doi.org/10.1016/j.nxener.2026.100581.

[5] R. Alayi, N. Khalilpoor, S. Heshmati, A. Najafi, A. Issakhov, Thermal and environmental analysis solar water heater System for residential buildings, Int. J. Photoenergy 2021 (2021) 6838138, https://doi.org/10.1155/2021/6838138.

[6] A. Greco, E. Gundabattini, D.S. Gnanaraj, C. Masselli, A comparative study on the performances of flat plate and evacuated tube collectors deployable in domestic solar water heating systems in different climate areas, Climate 8 (2020) 78, https://doi.org/10.3390/cli8060078.

[7] M.E. Soudani, K.E. Aiadi, D. Bechki, Water heating by Parabolic Trough Collector with storage in the Ouargla region of Algerian Sahara, Mater. Today Proc. 24 (2020) 137–139, https://doi.org/10.1016/j.matpr.2019.07.707.

[8] T. Maatallah, A. Houcine, S. El Alimi, S. Ben Nasrallah, A novel solar concentrating system based on a fixed cylindrical reflector and tracking receiver, Renew. Energy 117 (2018) 85–107, https://doi.org/10.1016/j.renene.2017.10.040.

[9] J. Mahdhi, F. Hamdi, H. Ebadi, A. Bouabidi, R. Ennetta, L. Savoldi, Experimental Study of a stationary parabolic trough collector with modified absorbers for domestic water heating, Energies 18 (2025) 3261, https://doi.org/10.3390/en18133261.

[10] M.V. Gustavo, P.R.C. Alberto, G.E.V. Hugo, G.V. Octavio, Methodology for obtaining instantaneous thermal performance curves for a parabolic trough solar by experimental data and projections based on a ray tracing model, Sol. Energy 262 (2023) 111827, https://doi.org/10.1016/j.solener.2023.111827.

[11] A. Kumar, S.K. Shukla, Thermal performance analysis of helical coil solar cavity receiver based parabolic trough concentrator, Therm. Sci. 23 (2019) 3539–3550, https://doi.org/10.2298/TSCI170830104K.

[12] E. Vengadesan, A.R. Ismail Rumaney, R. Mitra, S. Harichandan, R. Senthil, Heat transfer enhancement of a parabolic trough solar collector using a semicircular multitube absorber, Renew. Energy 196 (2022) 111–124, https://doi.org/10.1016/j.renene.2022.06.148.

[13] M. Halimi, I. Outana, J. Diouri, A. El Amrani, C. Messaoudi, Experimental investigation of absorbed flux circumferential distribution of an absorber with U-pipe tube exchanger for Parabolic Trough Collectors, Appl. Therm. Eng. 129 (2018) 1230–1239, https://doi.org/10.1016/j.applthermaleng.2017.10.075.

[14] M.A. Essa, M. Asal, M.A. Saleh, R.E. Shaltout, A comparative study of the performance of a novel helical direct flow U-Tube evacuated tube collector, Renew. Energy 163 (2021) 2068–2080, https://doi.org/10.1016/j.renene.2020.10.109.

[15] S. Gholipour, M. Afrand, R. Kalbasi, Improving the efficiency of vacuum tube collectors using new absorbent tubes arrangement: introducing helical coil and spiral tube adsorbent tubes, Renew. Energy 151 (2020) 772–781, https://doi.org/10.1016/j.renene.2019.11.068.

[16] S.N. Lotake, M.M. Wagh, Performance evaluation of multiple helical tubes as a receiver for solar parabolic trough collector, Asia Pacific J. Energy Environ. 7 (n. d.) 39–46. https://doi.org/10.18034/apjee.v7i1.272.

[17] S. Akbarzadeh, M.S. Valipour, The thermo-hydraulic performance of a parabolic trough collector with helically corrugated tube, Sustain. Energy Technol. Assessments 44 (2021) 101013, https://doi.org/10.1016/j.seta.2021.101013.

[18] O.P. Sunkarwar, B.K. Naik, A. Dasore, Experimental and Numerical study of parallel flow evacuated U-Tube solar collector with parabolic reflector: impact of particulate matter, J. Sol. Energy Eng. 147 (2025), https://doi.org/10.1115/1.4067664.

[19] B. Bayhan, G. Arslan, Experimental investigation of natural circulating solar energy system including a parabolic trough solar collector, J. Sol. Energy Eng. 147 (2024), https://doi.org/10.1115/1.4066301.

[20] V.M. Hameed, M. Abdulmjeed, M. Ali, Experimental and performance evaluation of a helical receiver in parabolic trough solar collectors, Arabian J. Sci. Eng. 51 (2026) 9179–9190, https://doi.org/10.1007/s13369-025-10627-7.

[21] N.K. Dengre, L. Yadav, A. Kumar, Experimental study of a newly design helical coil receiver in evacuated tube for parabolic trough solar reflector, J. Sol. Energy Eng. 148 (2026), https://doi.org/10.1115/1.4070919.

[22] A. Oumachtaq, M. Halimi, M. Ouhadou, Y. El Hassouani, M. Hajjaj, C. Messaoudi, Thermal performance evaluation of a parabolic trough collector receiver: a numerical study of three heat exchanger configurations, Case Stud. Therm. Eng. 72 (2025) 106303, https://doi.org/10.1016/j.csite.2025.106303.

[23] O. Chakraborty, S. Roy, B. Das, R. Gupta, Effects of helical absorber tube on the energy and exergy analysis of parabolic solar trough collector – a computational analysis, Sustain. Energy Technol. Assessments 44 (2021) 101083, https://doi.org/10.1016/j.seta.2021.101083.

[24] S. Said, S. Mellouli, T. Alqahtani, S. Algarni, R. Ajjel, New evacuated tube solar collector with parabolic trough collector and helical coil heat exchanger for usage in domestic water heating, Sustainability 15 (2023), https://doi.org/10.3390/su151511497.

[25] H. Ebadi, D.C. Alarcón-Padilla, R. Guedez, H. Mahmoudi, S. Trevisan, L. Valenzuela, L. Savoldi, Thermal design optimization of a parabolic trough collector receiver with a tube-bundle cavity, Sol. Energy 309 (2026) 114439, https://doi.org/10.1016/j.solener.2026.114439.

[26] J. Byiringiro, M. Chaanaoui, B. Hammouti, Enhancement of thermal performance in parabolic trough solar Collectors: investigation of three novel receiver configurations using advanced heat transfer fluids, Sol. Energy Mater. Sol. Cells 293 (2025) 113833, https://doi.org/10.1016/j.solmat.2025.113833.

[27] J. Mustafa, S. Alqaed, M. Sharifpur, Numerical study on performance of double-fluid parabolic trough solar collector occupied with hybrid non-Newtonian nanofluids: investigation of effects of helical absorber tube using deep learning, Eng. Anal. Bound. Elem. 140 (2022) 562–580, https://doi.org/10.1016/j.enganabound.2022.04.033.

[28] R. Loni, M. Sharifzadeh, Performance comparison of a solar parabolic trough concentrator using different shapes of linear cavity receiver, Case Stud. Therm. Eng. 60 (2024) 104603, https://doi.org/10.1016/j.csite.2024.104603.

[29] P. Saini, A. Dhar, S. Powar, Performance evaluation of a parabolic trough collector with a uniform helical wire coil flow insert, Results Eng. 21 (2024) 101794, https://doi.org/10.1016/j.rineng.2024.101794.

[30] X. Shi, X. Zhao, F. Wang, Z. Cheng, Y. Dong, J. Xu, Improving overall heat transfer performance of parabolic trough solar receiver by helically convex absorber tube, Appl. Therm. Eng. 213 (2022) 118690, https://doi.org/10.1016/j.applthermaleng.2022.118690.

[31] E. Bellos, C. Tzivanidis, Analytical expression of parabolic trough solar collector performance, Design 2 (2018) 9, https://doi.org/10.3390/designs2010009.

[32] R. Naveenkumar, M. Ravichandran, B. Stalin, A. Ghosh, A. Karthick, L.S.R.L. Aswin, S.S.H. Priyanka, S.P. Kumar, S.K. Kumar, Comprehensive review on various parameters that influence the performance of parabolic trough collector, Environ. Sci. Pollut. Res. Int. 28 (2021) 22310–22333, https://doi.org/10.1007/s11356-021-13439-y.

[33] R.E. Iliquin-Fernandez, J.J. Ligue-Tocas, F.I.E. Canaza, L.M. Mena-Chacon, M.Y. Chappa, P. Rituay, D. Mori-Mestanza, K.J. Vela-Vargas, C.M.O. Ramirez, M. A. Barrena-Gurbillón, Influence of absorber tube geometry on the thermal performance of a parabolic trough solar collector under heating cycles for hot water production, Next Energy 12 (2026) 100729, https://doi.org/10.1016/j.nxener.2026.100729.

[34] A.H. Al-Tohamy, O.A. Ismail, A. Kaood, Numerical investigation of the hydrothermal performance of convergent solar absorber with various corrugations fitted in a parabolic trough collector, Case Stud. Therm. Eng. 77 (2026) 107494, https://doi.org/10.1016/j.csite.2025.107494.

[35] C.S.L. Lim, S. Sobhansarbandi, A robust transient modeling approach for an energy storage-based concentrated solar thermal collector, Renew. Energy 256 (2026) 124360, https://doi.org/10.1016/j.renene.2025.124360.

[36] S. Kotak, N.J. Chotai, K. Motwani, Optimisation of a cut-tube absorber for parabolic trough collectors to minimise heat loss and pressure drop, Appl. Therm. Eng. 282 (2026) 128950, https://doi.org/10.1016/j.applthermaleng.2025.128950.

[37] M. Siavashi, M. Vahabzadeh Bozorg, M.H. Toosi, A numerical analysis of the effects of nanofluid and porous media utilization on the performance of parabolic trough solar collectors, Sustain. Energy Technol. Assessments 45 (2021) 101179, https://doi.org/10.1016/j.seta.2021.101179.

[38] D.N. Korres, T. Papingiotis, I. Koronaki, C. Tzivanidis, Thermal and optical analyses of a hybrid solar photovoltaic/thermal (PV/T) collector with asymmetric reflector: numerical modeling and validation with experimental results, Sustainability 15 (2023) 9932, https://doi.org/10.3390/su15139932.
[39] R.K. Donga, S. Kumar, G. Velidi, Heat transfer enhancement in a parabolic trough collector using finned tubular absorber, Sci. Rep. 15 (2025) 24142, https://doi.org/10.1038/s41598-025-07825-6.
[40] B. Li, X. Zhai, X. Cheng, Experimental and numerical investigation of a solar collector/storage system with composite phase change materials, Sol. Energy 164 (2018) 65–76, https://doi.org/10.1016/j.solener.2018.02.031.
[41] X. Randez, F. Sallaberry, A. Garcia de Jalon, O. Itoiz, Validation of a simulation method for the optical and thermal characterization on small-sized parabolic trough collector for process heat applications, Renew. Energy 256 (2026) 124562, https://doi.org/10.1016/j.renene.2025.124562.
[42] J. Byiringiro, M. Chaanaoui, M. Halimi, Heat transfer enhancement of a parabolic trough solar collector using innovative receiver configurations combined with a hybrid nanofluid: CFD analysis, Renew. Energy 233 (2024) 121169, https://doi.org/10.1016/j.renene.2024.121169.
[43] E. Bellos, C. Tzivanidis, Enhancing the performance of evacuated and non-evacuated parabolic trough collectors using twisted tape inserts, perforated plate inserts and internally finned absorber, Energies 11 (2018) 1129, https://doi.org/10.3390/en11051129.
[44] Z. Chen, X. Han, Y. Ma, Performance analysis of a novel direct absorption parabolic trough solar collector with combined absorption using MCRT and FVM coupled method, Renew. Energy 220 (2024) 119727, https://doi.org/10.1016/j.renene.2023.119727.
[45] E.M. Saleh, V.M. Hameed, Innovative new solar parabolic trough collector enhanced by corrugated receiver surface with PCM and turbulator inside, J. Energy Storage 86 (2024) 111403, https://doi.org/10.1016/j.est.2024.111403.
[46] M. Das, O. Pektezel, M. Sımsek, Solar energy for greenhouse drying: performance evaluation of parabolic trough solar collector with two-axis tracking system, Sol. Energy 299 (2025) 113716, https://doi.org/10.1016/j.solener.2025.113716.
[47] R.K. Donga, S. Kumar, G. Velidi, Numerical investigation of performance and exergy analysis in parabolic trough solar collectors, Sci. Rep. 14 (2024) 31908, https://doi.org/10.1038/s41598-024-83219-4.
[48] X. Xu, C. Wu, C. Liu, X. Xu, Feasibility assessment of trough concentrated solar power plants with transcritical power cycles based on carbon dioxide mixtures: a 4E analysis and systematic comparison, J. Clean. Prod. 436 (2024) 140603, https://doi.org/10.1016/j.jclepro.2024.140603.
[49] Z. Yang, W. Shi, D. Wang, F. Rong, Z. Yu, Energy, exergy, and exergoeconomic analysis of a novel integrated energy system based on parabolic trough solar collectors and LNG cold energy utilization, Int. J. Refrig. 180 (2025) 37–53, https://doi.org/10.1016/j.ijrefrig.2025.08.017.
[50] Y. Norouzghomi, A.A. Rabienataj Darzi, S.M. Mousavi, Heat transfer enhancement versus pressure drop penalties in a parabolic trough collector with a star-finned absorber tube, Int. Commun. Heat Mass Tran. 178 (2026) 111525, https://doi.org/10.1016/j.icheatmasstransfer.2026.111525.
[51] E. Bellos, I. Daniil, C. Tzivanidis, Multiple cylindrical inserts for parabolic trough solar collector, Appl. Therm. Eng. 143 (2018) 80–89, https://doi.org/10.1016/j.applthermaleng.2018.07.086.
[52] M. Wirz, J. Petit, A. Haselbacher, A. Steinfeld, Potential improvements in the optical and thermal efficiencies of parabolic trough concentrators, Sol. Energy 107 (2014) 398–414, https://doi.org/10.1016/j.solener.2014.05.002.
[53] H. Ebadi, A. Cammi, N. Fathi, L. Savoldi, Heat transfer enhancement on CSP tubular receivers using partially filled Raschig Ring porous inserts: a numerical study, Sol. Energy 297 (2025) 113635, https://doi.org/10.1016/j.solener.2025.113635.
[54] R.T. AbdelFatah, R. Shalaby, I.S. Fahim, M.M. Kasem, Optimized control, and experimental validation of a novel multi-stage parabolic trough collector for solar water heating systems, Sci. Rep. 16 (2026) 3054, https://doi.org/10.1038/s41598-025-34564-5.
[55] M.O. Karaağaç, B. Akıncı, A. Ergün, Enhancing the performance of parabolic trough solar collectors: Cost-effective innovative designs for sustainable energy harvesting, Appl. Therm. Eng. 253 (2024) 123693, https://doi.org/10.1016/j.applthermaleng.2024.123693.
[56] S. Baharloui, M.M. Peiravi, M.G. bandpy, Thermal optimization and exergy efficiency of two new parabolic solar collectors using response surface methodology, Results, Chem 13 (2025) 101984, https://doi.org/10.1016/j.rechem.2024.101984.
[57] E.G. Barbosa, M.A. Martins, M.E. Viana de Araujo, N. dos S. Renato, S. Zolnier, E.G. Pereira, M. de Oliveira Resende, Experimental evaluation of a stationary parabolic trough solar collector: influence of the concentrator and heat transfer fluid, J. Clean. Prod. 276 (2020), https://doi.org/10.1016/j.jclepro.2020.124174.